Article

Cell

Light Controls Protein Localization through Phytochrome-Mediated Alternative Promoter Selection

Graphical Abstract

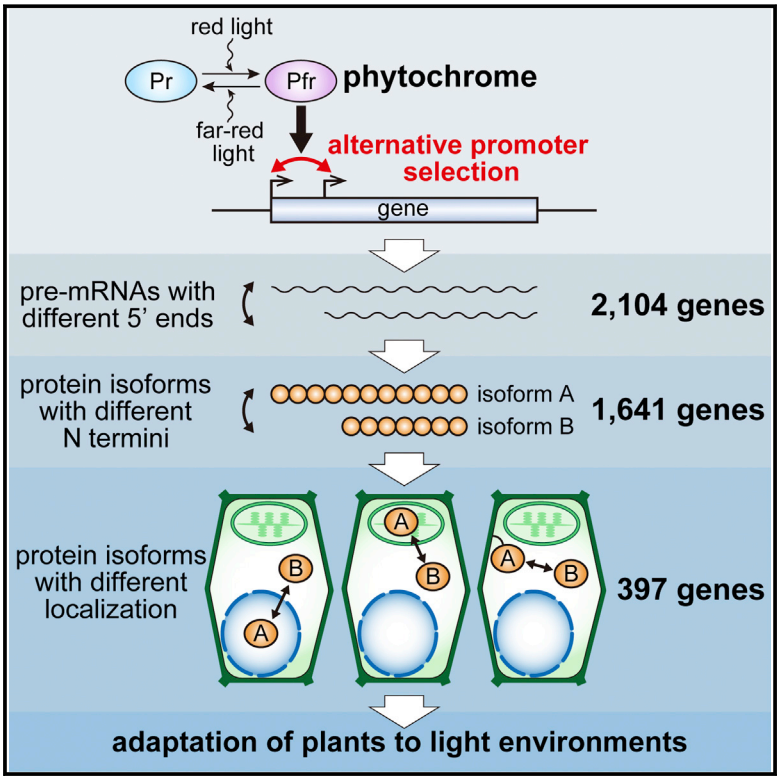

Authors

Tomokazu Ushijima, Kousuke Hanada, Eiji Gotoh, ..., Yasuomi Tada, Yutaka Suzuki, Tomonao Matsushita

Correspondence

mat@agr.kyushu-u.ac.jp

In Brief

Light signaling through phytochrome receptors changes protein localization through alternative promoter selection, allowing plants to metabolically respond to changing light conditions.

Highlights

- Phytochrome induces genome-wide changes in alternative promoter selection
- Phytochrome-mediated alternative promoter selection modulates protein localization
- This mechanism produces a cytoplasmic isoform of glycerate kinase (cytGLYK)
- cytGLYK accumulates in shade to alleviate fluctuating light-induced photoinhibition

Data Resources

DRA005891

Ushijima et al., 2017, Cell *171*, 1316–1325
November 30, 2017
https://doi.org/10.1016/j.cell.2017.10.018

CellPress

Cell

Article

Light Controls Protein Localization through Phytochrome-Mediated Alternative Promoter Selection

Tomokazu Ushijima,[1,13] Kousuke Hanada,[2,3,13] Eiji Gotoh,[1] Wataru Yamori,[4,5] Yutaka Kodama,[6] Hiroyuki Tanaka,[6] Miyako Kusano,[5,7,8] Atsushi Fukushima,[8] Mutsutomo Tokizawa,[9] Yoshiharu Y. Yamamoto,[9,10] Yasuomi Tada,[11] Yutaka Suzuki,[12] and Tomonao Matsushita[1,5,14,*]

[1]Faculty of Agriculture, Kyushu University, Fukuoka 812-8581, Japan
[2]Department of Bioscience and Bioinformatics, Kyushu Institute of Technology, Fukuoka 820-8502, Japan
[3]CREST, JST, Saitama 332-0012, Japan
[4]Graduate School of Science, The University of Tokyo, Tokyo 113-0033, Japan
[5]PRESTO, JST, Saitama 332-0012, Japan
[6]Center for Bioscience Research and Education, Utsunomiya University, Tochigi 321-8505, Japan
[7]Graduate School of Life and Environmental Sciences, University of Tsukuba, Ibaraki 305-8572, Japan
[8]RIKEN Center for Sustainable Resource Science, Kanagawa 230-0045, Japan
[9]United Graduate School of Agricultural Science, Gifu University, Gifu 501-1103, Japan
[10]Faculty of Applied Biological Sciences, Gifu University, Gifu 501-1103, Japan
[11]Center for Gene Research, Nagoya University, Aichi 464-8602, Japan
[12]Graduate School of Frontier Sciences, The University of Tokyo, Chiba 277-8562, Japan
[13]These authors contributed equally
[14]Lead Contact
*Correspondence: mat@agr.kyushu-u.ac.jp
https://doi.org/10.1016/j.cell.2017.10.018

SUMMARY

Alternative promoter usage is a proteome-expanding mechanism that allows multiple pre-mRNAs to be transcribed from a single gene. The impact of this mechanism on the proteome and whether it is positively exploited in normal organismal responses remain unclear. We found that the plant photoreceptor phytochrome induces genome-wide changes in alternative promoter selection in *Arabidopsis thaliana*. Through this mechanism, protein isoforms with different N termini are produced that display light-dependent differences in localization. For instance, shade-grown plants accumulate a cytoplasmic isoform of glycerate kinase (GLYK), an essential photorespiration enzyme that was previously thought to localize exclusively to the chloroplast. Cytoplasmic GLYK constitutes a photorespiratory bypass that alleviates fluctuating light-induced photoinhibition. Therefore, phytochrome controls alternative promoter selection to modulate protein localization in response to changing light conditions. This study suggests that alternative promoter usage represents another ubiquitous layer of gene expression regulation in eukaryotes that contributes to diversification of the proteome.

INTRODUCTION

Biological complexity relies on the diversity of the proteome. Higher organisms expand their coding capacity via various mechanisms. Whereas alternative splicing involves different combinations of exons in a gene being spliced together to form different mRNA variants, alternative promoter usage results in multiple pre-mRNAs being transcribed from different transcription start sites (TSSs) within a gene locus (Davuluri et al., 2008; Landry et al., 2003). The patterns of alternative promoter selection are altered in different organs/tissues and in cancer cells (Barrera et al., 2008; Mejía-Guerra et al., 2015; Tsuchihara et al., 2009; Wiesner et al., 2015). In most cases, alternative promoter selection generates alterations in 5′ UTR sequences that can affect the translational efficiency or stability of mRNA (Mejía-Guerra et al., 2015; Rojas-Duran and Gilbert, 2012; Wang et al., 2016). In a limited number of cases, alternative promoter selection appears to alter the N-terminal lengths of the encoded proteins (Davuluri et al., 2008; Landry et al., 2003; Mejía-Guerra et al., 2015; Wiesner et al., 2015). However, it remains largely unknown to what extent this mechanism contributes to diversification of the proteome, and whether it represents a ubiquitous aspect of signal transduction in normal organismal responses to stimuli.

Light, the energy source of photosynthesis, is a very important environmental signal obtained by plants. Plants constantly monitor ambient light conditions through several sensory photoreceptors, such as phytochromes, and modulate their morphology and metabolism to adapt to fluctuating environmental conditions and to optimize photosynthesis (Franklin and Quail, 2010; Galvão and Fankhauser, 2015). Phytochromes are reversibly activated and inactivated by the absorption of red and far-red light, respectively, which enables plants to sense the red/far-red light ratio in the environment (Casal, 2013; Franklin and Quail, 2010; Galvão and Fankhauser, 2015). Upon absorption of red light, activated phytochromes are translocated from

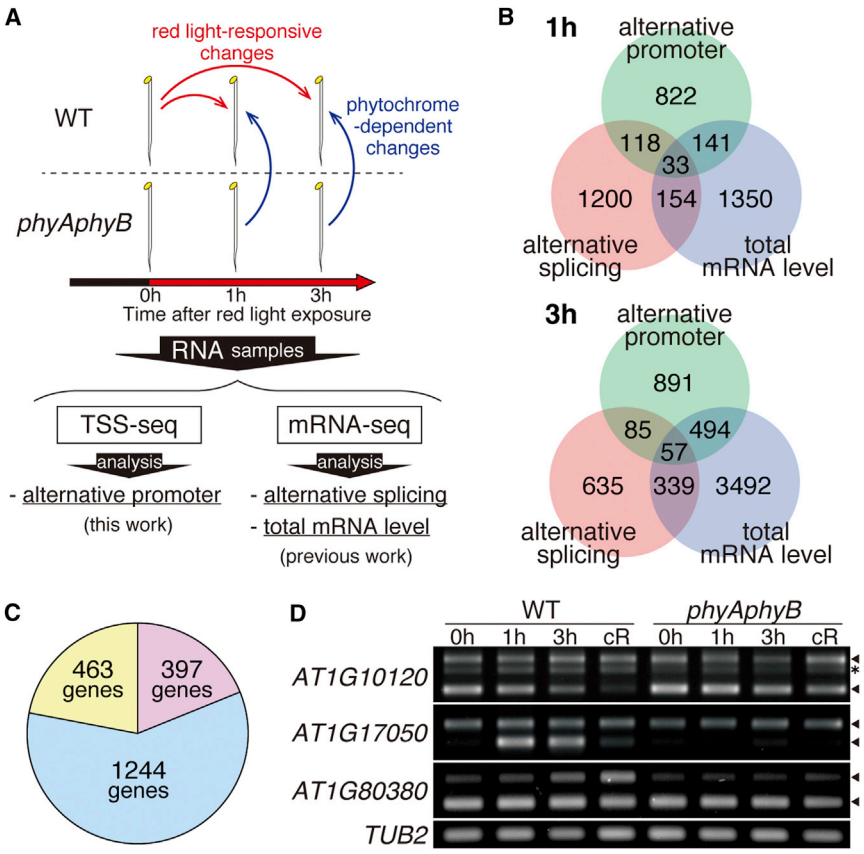

Figure 1. Phytochrome Controls Genome-wide Alternative Promoter Selection in *Arabidopsis*

(A) Experimental design of the TSS-seq analysis. Total RNA was extracted from 4-day-old wild-type (WT) and *phyAphyB* double mutant etiolated seedlings that were exposed to continuous red light (cR) (8.3 μmol m^{-2} s^{-1}) for 0, 1, or 3 hr.

(B) Venn diagrams showing the number of genes that exhibited phytochrome-regulated changes in alternative promoter usage, alternative splicing, or total transcript level, at 1 and 3 hr after red light exposure.

(C) Estimated impact on the proteome at 1 and/or 3 hr after exposure to red light. The number of genes that show protein localization change (red), protein sequence change without localization change (blue), or no change in protein sequence (yellow) is shown.

(D) Validation by 5′ RACE analysis. The same RNA samples as in (A) and those from seedlings grown in cR were analyzed. Arrowheads indicate transcripts identified in the TSS-seq analysis as exhibiting phytochrome-regulated alternative promoter selection. Asterisk indicates nonspecific band. *TUB2* was used as an internal control.

See also Figures 2 and S1, Tables S1–S6, and Data S1.

the cytoplasm to the nucleus, where they inhibit the activity of several transcription factors, and thereby induce genome-wide changes in the transcription of target genes and mediate various light responses (Leivar and Monte, 2014; Menon et al., 2016).

Recently, by performing mRNA sequencing (mRNA-seq) analysis of red-light-responsive and phytochrome-dependent transcriptomic changes during seedling de-etiolation, we found that phytochrome controls not only transcription, but also alternative splicing, at a similar genomic scale, to mediate light responses in *Arabidopsis thaliana* (Shikata et al., 2014). Light-regulated alternative splicing has also been reported in similar mRNA-seq analyses, not only in *Arabidopsis* (Hartmann et al., 2016; Mancini et al., 2016) but also in the moss *Physcomitrella* (Wu et al., 2014). Some alternative splicing events can be attributed to TSS changes caused by alternative promoter selection, because alternative promoter-mediated inclusion or exclusion of the 5′ end sequences of pre-mRNA can affect subsequent alternative splicing patterns (Kornblihtt, 2005; Shabalina et al., 2010). Therefore, we reasoned that phytochrome might also directly regulate alternative promoter selection.

RESULTS AND DISCUSSION

Phytochrome Induces Genome-wide Changes in Alternative Promoter Selection in *Arabidopsis*

To investigate the possibility that phytochrome controls alternative promoter selection, we performed TSS sequencing (TSS-seq) analysis. In this technique, after the adaptor sequence is directly introduced to the 5′ cap structure of mRNA, only the 5′ end sequences of mRNA are analyzed by a massively parallel sequencer to determine the precise positions and expression levels of all the TSSs in the genome (Tsuchihara et al., 2009). For the TSS-seq analysis, we used the same RNA samples as those in the previous mRNA-seq analysis, which were extracted from red-light-exposed, etiolated wild-type, and mutant seedlings deficient in both phytochrome A (phyA) and phyB (Shikata et al., 2014) (Figure 1A; Table S1). These experimental conditions were chosen to analyze direct effects of phytochrome signals on the transcriptome, because phytochrome mutation causes no morphological changes in etiolated seedlings, and because phyA and phyB are the dominant members of the phytochrome family that function in a partially redundant manner in this condition (Franklin and Quail, 2010).

We mapped TSS-seq reads to the *Arabidopsis* genome and found that they were enriched in the annotated representative TSSs of each coding gene (Figure S1A). The inferred transcript levels significantly correlated with those determined by our previous mRNA-seq analysis under all conditions tested ($0.69 < \text{correlation coefficient} < 0.76$, $p < 2.2 \times 10^{-16}$) (Figure S1B). We identified 40,709 non-redundant TSS peaks (hereafter referred to as TSSs) (Figure S1C), including 13,819 that overlapped with representative TSSs in annotated genes. Of the remaining 26,890 TSSs, 16,754 were novel TSSs of unannotated genes, and 10,136 were non-representative TSSs of 6,143 annotated genes that potentially have alternative promoters. To identify phytochrome-regulated alternative

promoter selection, we detected red-light-responsive and phytochrome-dependent changes in the ratio of TSS-seq reads among each alternative TSS pair (Figure S1D). Using this approach, we identified 5,644 phytochrome-regulated changes in alternative promoter selection in 2,104 genes, after 1 hr and/or 3 hr of exposure of etiolated seedlings to continuous red light (Figure 1B; Data S1).

We compared these TSS-seq results with our previous mRNA-seq analysis of red-light-responsive and phytochrome-dependent changes in alternative splicing patterns or total transcript levels (Shikata et al., 2014). Interestingly, 1,114 genes showed phytochrome-dependent, rapid changes in alternative promoter selection within 1 hr of red light exposure, while only 14% of these genes showed phytochrome-regulated alternative splicing (Figure 1B), indicating that phytochrome is directly involved in the genome-wide regulation of alternative promoter selection. Since alternative promoter selection is a transcriptional regulatory mechanism, we expected that alternative promoter selection would generally be associated with changes in total transcript levels. However, surprisingly, 84% of the genes under the control of phytochrome-mediated alternative promoter selection did not show any significant changes in total mRNA levels within 1 hr of red light exposure (Figure 1B). Probes for microarray analysis are usually designed around the 3′ end of each gene. A focus on measuring mRNA abundance with 3′ probes most likely explains why changes in alternative promoter selection have gone undetected.

Finally, we found that genes directly bound by phyB (Jung et al., 2016) were significantly enriched in the 2,104 genes showing phytochrome-mediated alternative promoter selection, as well as in the 5,096 genes with phytochrome-regulated changes in total mRNA levels within 1 hr and/or 3 hr of red light exposure (Table S2), indicating that phyB directly regulates alternative promoter selection in target promoters.

Phytochrome-Mediated Alternative Promoter Selection Modulates Subcellular Localization of a Number of Proteins

To examine the functional impact of phytochrome-controlled alternative promoter selection, we searched for cases where the N-terminal lengths of the encoded proteins were altered. When we looked only at proteins for which the reading frame was not altered, we found that 1,641 of the 2,104 genes that are regulated by phytochrome-mediated alternative promoter selection encode multiple protein isoforms with different N termini, where shorter protein isoforms with N-terminal truncations are produced from alternative promoters in most of the cases (1,636/1,641 genes) (Data S1). Moreover, the protein isoforms encoded by 397 of these 1,641 genes were predicted, based on a software (King and Guda, 2007), to have different subcellular localizations (Figure 1C; Data S1), suggesting that the subcellular localization of proteins is globally modulated by light through phytochrome-mediated alternative promoter selection.

Gene ontology (GO) analysis showed that a number of plastid/chloroplast- or photosynthesis-related GO terms were significantly enriched, both among the 397 genes (Table S3) and among the 1,641 genes (Table S4). Furthermore, the proportion of genes predicted to encode plastidial proteins with N-terminal transit peptides was significantly higher among the 1,641 genes than among all of the other annotated coding genes (Table S5). Therefore, phytochrome-controlled alternative promoter selection appears to affect subcellular localization signals for a variety of plastidial proteins.

To validate the TSS-seq data, we manually selected 100 genes from the 2,104 genes based on the designability of specific primers with no off-target annealing, and subjected these genes to 5′ rapid amplification of cDNA ends (5′ RACE) analysis. Both of the longer and shorter transcripts from alternative promoters were detected only for 30 of the 100 genes, probably because 5′ RACE is intrinsically less sensitive than TSS-seq (Tsuchihara et al., 2009). We then confirmed phytochrome-regulated significant changes in alternative promoter selection for 20 of the 30 genes (Figures 1D and 2; Table S6). For each of the 20 validated genes, we cloned longer and shorter cDNAs derived from different TSSs determined by the 5′ RACE experiments and expressed them as fusion proteins with GFP in onion epidermal cells and *Arabidopsis* mesophyll protoplasts. Confocal microscopy analysis showed that the longer and shorter cDNAs encoded protein isoforms with different subcellular localizations for six of the 20 genes (Figures 3 and S2). Whereas all of the shorter protein isoforms were localized to the cytoplasm, the longer isoforms localized to various subcellular compartments, including plastids (*AT1G80380*, *AT3G02040*, *AT4G34120*, and *AT5G44650*), the nucleus (*AT5G53930*), and the plasma membrane (*AT4G04960*) (Figures 3 and S2). Consistent with the GO and transit peptide-prediction results (Tables S3, S4, and S5), four of the six genes encoded plastid-localized, longer isoforms.

GLYK Shows Light-Dependent Changes in Subcellular Localization *In Vivo*

One of these four genes, *AT1G80380*, encodes glycerate kinase (GLYK), a photorespiratory enzyme that was previously thought to localize only to the chloroplast (Boldt et al., 2005). However, we found that, whereas *AT1G80380* expresses a longer mRNA that encodes plastid-localized GLYK (ptGLYK) in the light, it also expresses a shorter mRNA in darkness that encodes cytoplasmic GLYK (cytGLYK) with truncation of the N-terminal transit peptide (Figures S3A and S3B). *AT1G80380* also displays phytochrome-regulated alternative splicing, probably due to changes in alternative promoter selection (Figure S3).

To verify the light-dependent changes in the subcellular localization of GLYK proteins *in vivo*, we generated transgenic *Arabidopsis* plants transformed with the *GLYK* genomic fragment fused to *GFP* in the *glyk*-null mutant background (gGLYK-GFP line) (see the STAR Methods). We also generated two control lines in the *glyk* mutant background: the ptGLYK-GFP line, in which the second ATG was mutated in the *gGLYK-GFP* construct to accumulate only ptGLYK proteins, and the cytGLYK-GFP line, which constitutively expresses cytGLYK-GFP fusion proteins (see the STAR Methods). Regardless of the light conditions, the ptGLYK-GFP and cytGLYK-GFP lines showed GFP fluorescence only in the chloroplast and cytoplasm, respectively. By contrast, the gGLYK-GFP line showed

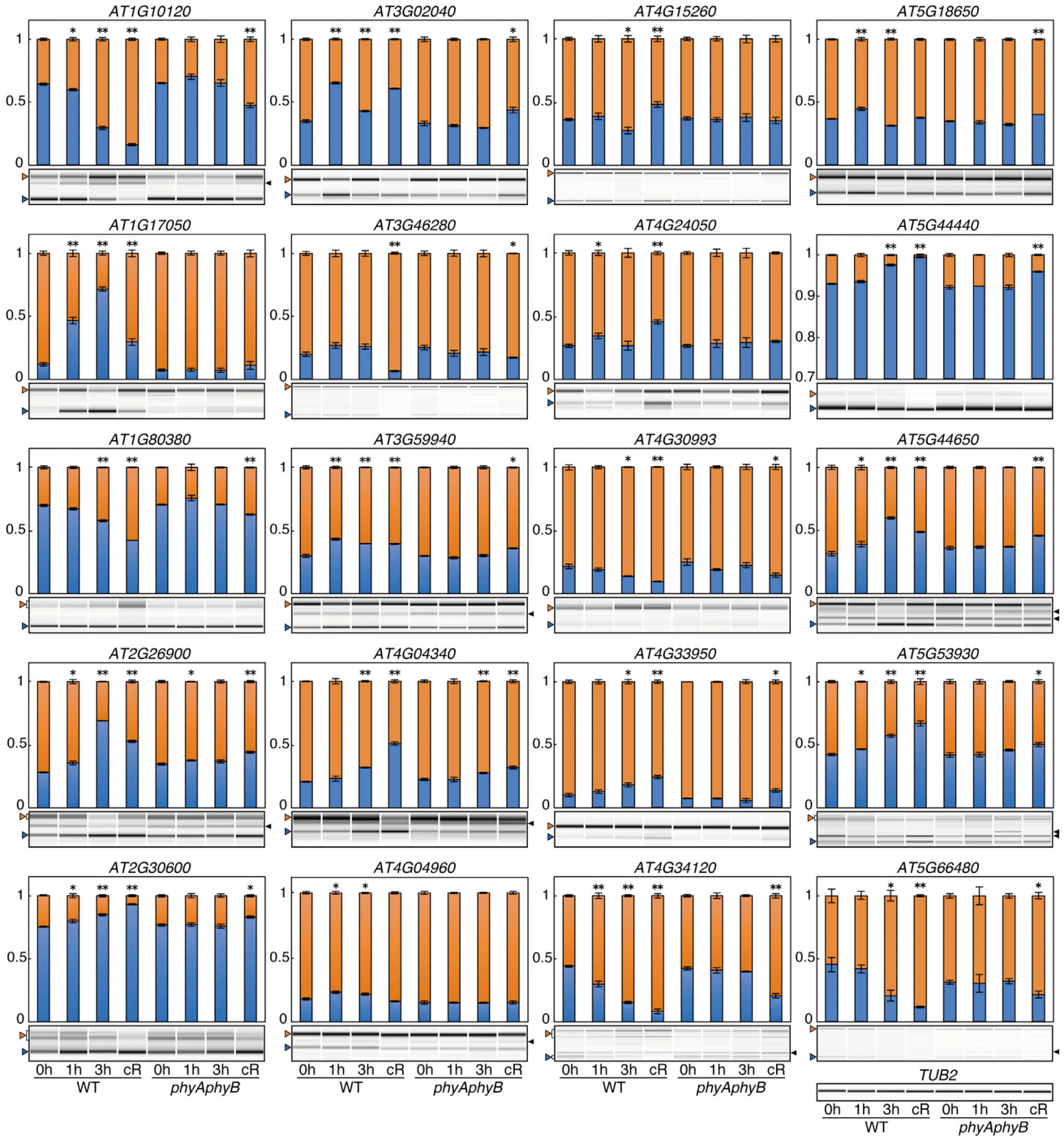

Figure 2. Validation of Phytochrome-Regulated Alternative Promoter Selection

The same RNA samples as in Figure 1D were analyzed by 5′ RACE, and the amounts of transcripts from phytochrome-controlled alternative promoters were quantified using an Agilent 2100 Bioanalyzer. The ratio between the longer (red) and shorter (blue) transcripts in each sample is shown. Data are means of technical replicates ±SE (n = 3). Asterisks show statistical significance of the shorter transcript ratio compared to the respective dark value at 0 hr, as determined by Student's t test (*p < 0.05, **p < 0.01). The bottom panels show representative gel-like images obtained using the Bioanalyzer. Red and blue arrowheads indicate quantified specific bands for the longer and shorter transcripts, respectively. The specific bands were confirmed by sequencing all the bands in each reaction. Black arrowheads indicate nonspecific bands. *TUB2* is shown as a loading control. See also Figure 1D and Table S6.

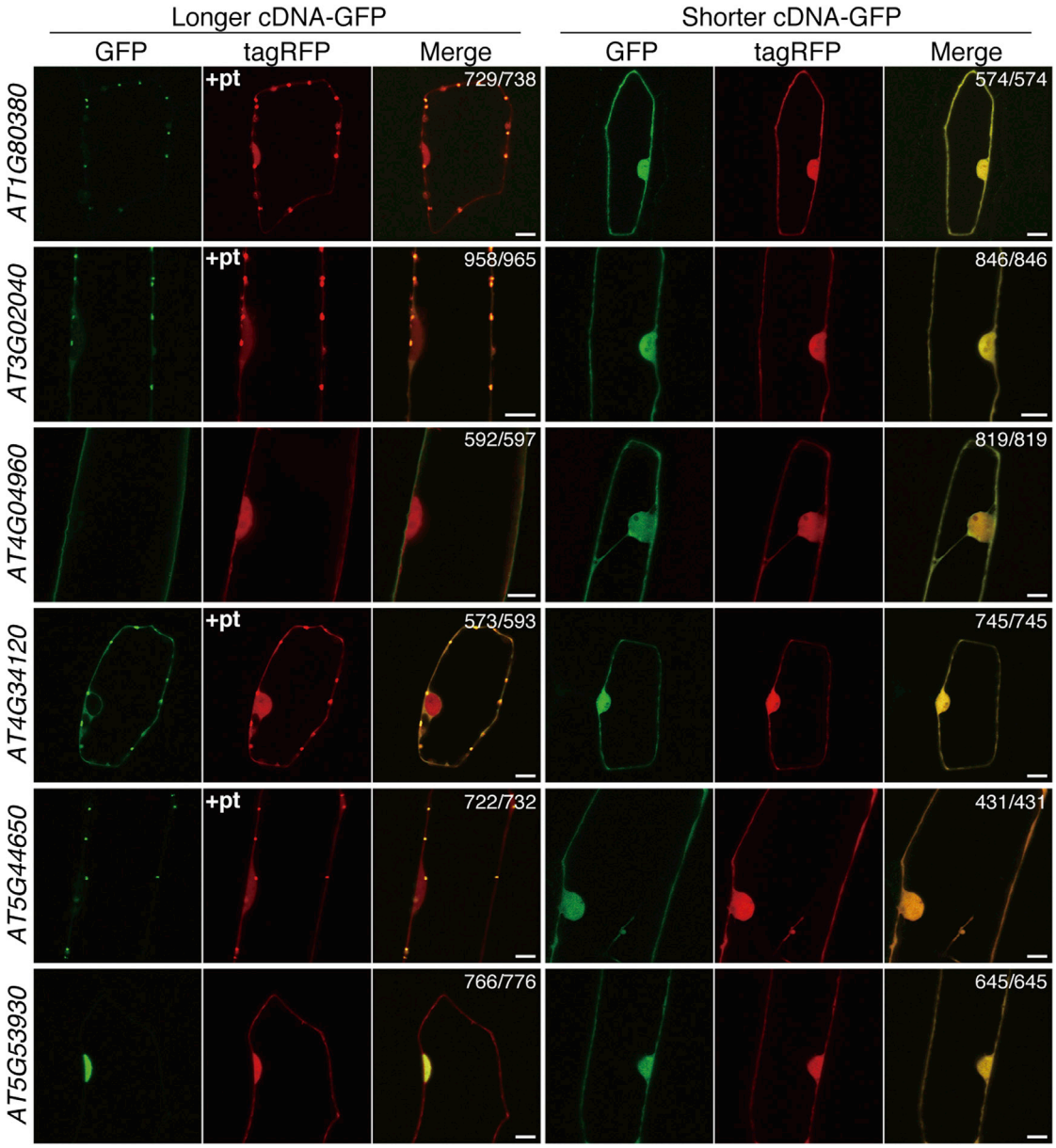

Figure 3. Phytochrome-Mediated Alternative Promoter Selection Produces Protein Isoforms that Are Localized to Different Regions of the Cell

Longer and shorter cDNAs resulting from phytochrome-mediated alternative promoter selection were expressed as fusion proteins with GFP in onion epidermal cells. tagRFP alone was co-expressed to label the cytoplasm and nucleus. In some samples, tagRFP fused to plastid transit peptide was additionally co-expressed to indicate plastids (+pt). The number of cells showing respective localization pattern of GFP per number of cells observed is shown. Scale bars, 20 μm. See also Figure S2.

cytoplasmic GFP fluorescence only in darkness, in addition to constitutive chloroplastic signals (Figures 4A and S4). These results indicate that GLYK proteins indeed show light-dependent changes in subcellular localization.

To further verify this observation immunochemically, we generated an anti-cytGLYK antibody that specifically recognizes cytGLYK and an anti-totalGLYK antibody that detects both ptGLYK and cytGLYK (Figure 4B). Anti-cytGLYK antibodies detected a major band of the predicted size only in the chloroplast-excluded fraction from cytGLYK-GFP plants, whereas anti-totalGLYK antibodies recognized bands of a similar size in both the chloroplast fraction from the ptGLYK-GFP line and the chloroplast-excluded fraction from the cytGLYK-GFP line (Figure 4C), demonstrating the specificity of each antibody. Immunoblot analysis with these antibodies showed that the gGLYK-GFP line accumulated cytGLYK-GFP proteins only in darkness, but accumulated ptGLYK-GFP proteins in both light and darkness (Figure 4D). Thus, light-dependent changes in

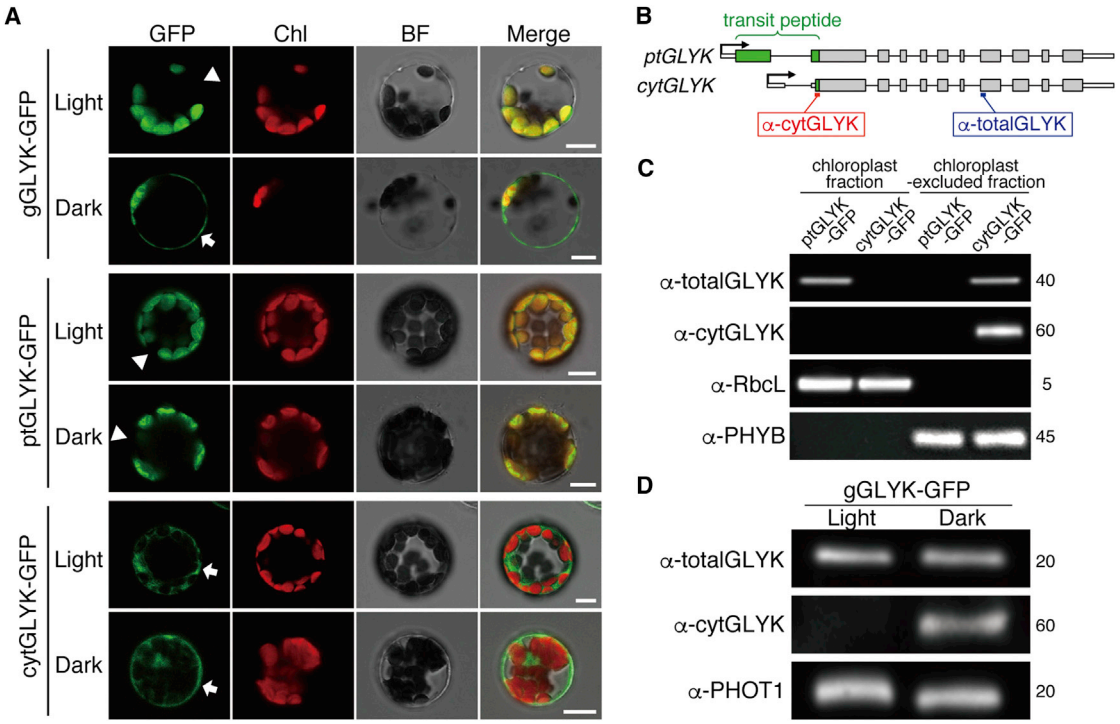

Figure 4. Light-Dependent Changes in the Subcellular Localization of GLYK Proteins *In Vivo*

(A) Subcellular localization of GFP fluorescence in the mesophyll protoplasts of gGLYK-GFP, ptGLYK-GFP, and cytGLYK-GFP transgenic plants grown in continuous white light (70 μmol m^{-2} s^{-1}) and dark conditions. Arrows and arrowheads indicate the presence and absence of cytoplasmic GFP fluorescence, respectively. Chl, chlorophyll autofluorescence; BF, bright field. Scale bars, 10 μm.

(B) Antibodies that recognize both ptGLYK and cytGLYK (α-totalGLYK) or only cytGLYK (α-cytGLYK) were generated. The epitope-encoding region of each antibody is shown in the schematic illustration of *ptGLYK* and *cytGLYK* pre-mRNAs.

(C) The chloroplast and chloroplast-excluded fractions of ptGLYK-GFP and cytGLYK-GFP transgenic plants were analyzed by immunoblot with anti-totalGLYK and anti-cytGLYK antibodies. Anti-RbcL and anti-PHYB antibodies were used as controls for fractionation.

(D) Immunoblot analysis using anti-totalGLYK and anti-cytGLYK antibodies. Anti-PHOT1 antibody was used for loading controls. Total protein was extracted from the shoots of light-grown 2-week-old gGLYK-GFP 2-7 transgenic plants (see Figure S5A) with or without 1 day of dark adaptation before sampling. The amount of total protein loaded in each lane (in micrograms) is indicated on the right in (C) and (D).

See also Figures S3 and S4.

GLYK localization were confirmed *in vivo* using two different techniques, demonstrating that light modulates the subcellular localization of a protein through phytochrome-mediated alternative promoter selection. These results also suggest that GLYK fulfills an additional function in the cytoplasm.

cytGLYK Constitutes a Cytoplasmic Bypass of Photorespiration

GLYK, which is encoded by a single gene in *Arabidopsis*, is an essential enzyme in the photorespiratory cycle that rapidly metabolizes 2-phosphoglycolate (2PG), a highly toxic product of the oxygenase activity of ribulose-1,5-bisphosphate-carboxylase/oxygenase (Rubisco), and returns its carbon to the Calvin cycle (Peterhansel et al., 2010) (Figure 5A). GLYK catalyzes the conversion of glycerate to 3-phosphoglycerate (3PGA) during the final step of photorespiration in the chloroplast (Boldt et al., 2005; Peterhansel et al., 2010). Whereas the *glyk* mutation is lethal in ambient air due to a complete block of the photorespiratory cycle, which leads to an overaccumulation of 2PG (Boldt et al., 2005), gGLYK-GFP and ptGLYK-GFP plants in this background showed normal growth, as expected (Figure 5B). Unexpectedly, the cytGLYK-GFP plants also survived in ambient air (Figure 5B), although this line accumulated only cytGLYK protein in the cytoplasm (Figures 4A, 4C, and S4). Under high CO_2 conditions, all lines exhibited normal growth, since the oxygenase activity of Rubisco (which produces 2PG) is inhibited under this condition (Boldt et al., 2005; Peterhansel et al., 2010) (Figure 5B). These observations were confirmed by measuring the fresh weight in independent transgenic lines for each construct (Figures 5C and S5A). We further showed that, while the CO_2 uptake in response to light was significantly reduced in the *glyk* mutant as previously reported (Takahashi et al., 2007), cytGLYK-GFP partially rescued this phenotype (Figure S5B). Since no GLYK protein was detected in the chloroplast fraction of the cytGLYK-GFP plants (Figure 4C), these results indicate that, in the absence of ptGLYK, cytGLYK alone drives photorespiration in the cytoplasm to detoxify 2PG.

Hydroxypyruvate (Hpyr), a membrane-permeable photorespiratory intermediate, can diffuse out of the peroxisome to the

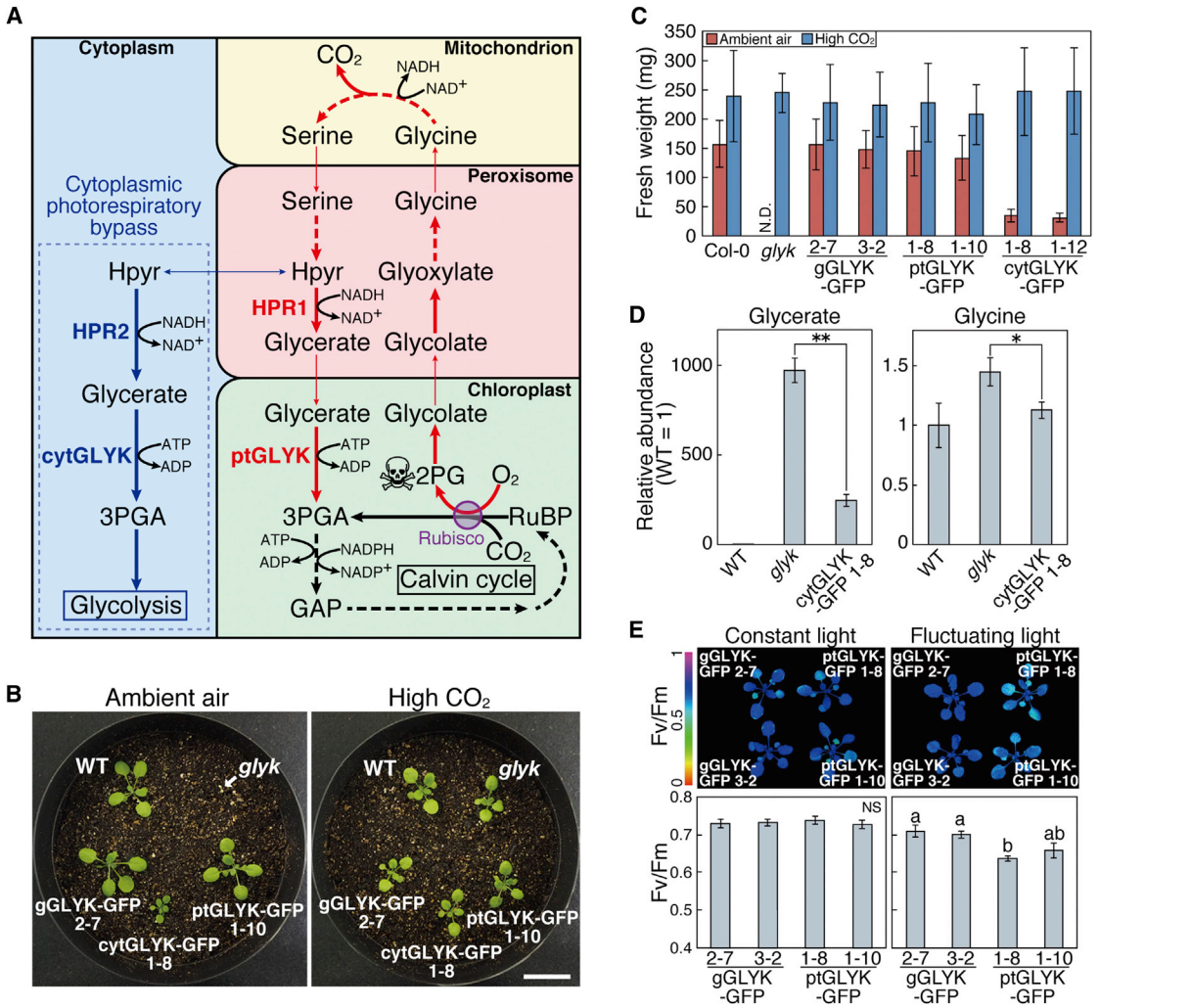

Figure 5. cytGLYK Constitutes Cytoplasmic Bypass of Photorespiration to Alleviate Fluctuating Light-Induced Photoinhibition

(A) Model of cytoplasmic photorespiratory bypass (in blue) and the conventional photorespiratory pathway (in red).

(B) Mature plants grown for 3 weeks under continuous white light (120 μmol m^{-2} s^{-1}) in ambient air or high CO_2 (0.2%) conditions. Scale bar, 2 cm.

(C) Fresh weight of mature plants grown for 4 weeks under continuous white light (120 μmol m^{-2} s^{-1}) in ambient air or high CO_2 (0.2%) conditions. Data are means ± SD (n = 8). N.D., not determined.

(D) Accumulation of photorespiratory metabolites. Plants were grown in high CO_2 (0.2%) conditions for 2 weeks and then shifted to ambient air for 2 min before the shoot tissues were sampled. Data are means ± SD of three independent biological replicates. *$p < 0.05$, **$p < 0.001$ (Welch's t test).

(E) The degree of photoinhibition was analyzed after irradiating the plants with constant high light (12-hr light/12-hr dark) or fluctuating light (3-min light/5-min dark) at 550 μmol m^{-2} s^{-1} for 2 days. Data are means ± SD (n = 3). Different letters indicate significantly different values ($p < 0.05$, Tukey-Kramer multiple comparison test). NS, not significant.

See also Figure S5.

cytoplasm, where it is converted into glycerate by hydroxypyruvate reductase 2 (HPR2), a cytoplasmic paralog of peroxisomal HPR1 (Timm et al., 2008). Subsequently, cytGLYK might convert the cytoplasmic glycerate into 3PGA, at least some of which would be metabolized via glycolysis (Figure 5A). To verify this possibility, we measured the levels of not only glycerate but also glycine, because glycine is a photorespiratory intermediate that shows the most prominent increase in *hpr1* mutants compared to wild-type plants (Timm et al., 2008). We found that these photorespiratory intermediates accumulated at significantly lower levels in cytGLYK-GFP plants than in the *glyk* mutant (Figure 5D). In the *glyk* mutant, the photosynthetic rate began to decrease within 5 min of transfer from high CO_2 to normal air conditions (Figure S5C), and severe photoinhibition was observed 24 hr after the transfer (Figure S5D). These atmosphere condition-specific defects resulting from arrested photorespiration were partially recovered in the cytGLYK-GFP lines (Figures S5C and S5D), indicating that the photorespiratory pathway was active in cytGLYK-GFP plants. Taken together, these data indicate that cytGLYK can drive photorespiration in the cytoplasm, strongly suggesting the existence of cytoplasmic photorespiratory bypass.

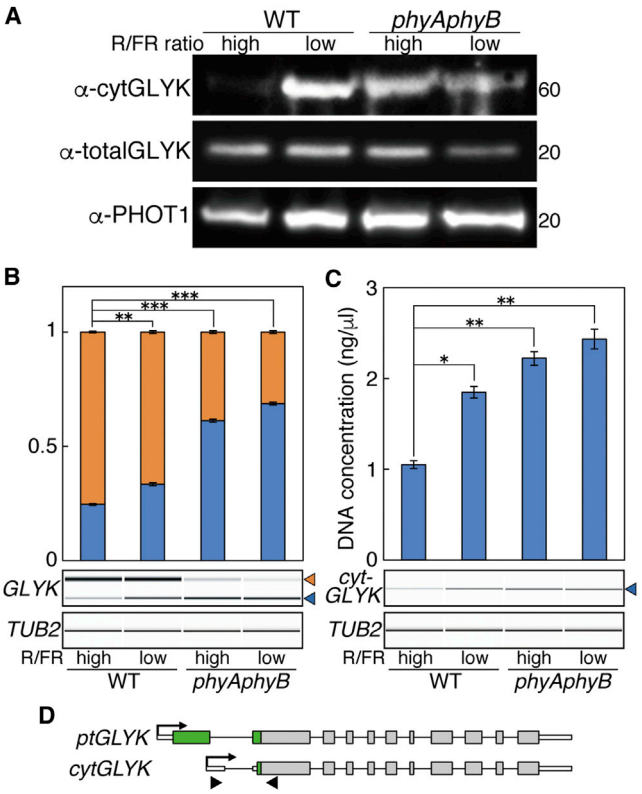

Figure 6. cytGLYK Accumulates in Response to Shade through Phytochrome-Mediated Alternative Promoter Selection

(A) Accumulation of endogenous cytGLYK proteins in WT and *phyAphyB* seedlings grown in high-red/far-red (R/FR) light (R/FR = 3) and low R/FR light (simulated shade: R/FR = 0.3) conditions for 4 days. Details are as in Figure 4D. The amount of total protein loaded in each lane (in micrograms) is indicated on the right.

(B–D) 5′ RACE analysis of *GLYK* (B) and RT-PCR analysis of *cytGLYK* (C and D) using the same samples as in (A). In (B), the ratio between *ptGLYK* (red) and *cytGLYK* (blue) transcripts is shown. In (C), *cytGLYK* transcripts were amplified using the *cytGLYK*-specific primers that are indicated by black arrowheads in (D), and the RT-PCR products were quantified with the Bioanalyzer. Data are means ± SE of three independent biological replicates. Asterisks show statistical significance of the *cytGLYK* ratio (B) or *cytGLYK* transcript level (C), compared to the value of WT samples in the high R/FR light condition, as determined by Student's t test (*$p < 0.001$, **$p < 0.0005$, ***$p < 0.000005$). The bottom panels show representative gel-like images obtained using the Bioanalyzer. Red and blue arrowheads indicate quantified bands for *ptGLYK* and *cytGLYK*, respectively. *TUB2* is shown as a loading control.

See also Figures 2 and S3 and Table S6.

cytGLYK Accumulates in Response to Shade and Alleviates Fluctuating Light-Induced Photoinhibition

Because cytoplasmic photorespiratory bypass could be used to metabolize 2PG without using chloroplastic ATP (Figure 5A), this process might increase the ATP/NADPH ratio in the chloroplast, which is required for alleviating photoinhibition in plants irradiated with fluctuating light levels (Suorsa et al., 2012; Yamori and Shikanai, 2016). Therefore, we examined whether cytGLYK affects photoinhibition in plants subjected to fluctuating light conditions. Although we did not detect any difference between cytGLYK-deficient ptGLYK-GFP lines and gGLYK-GFP lines under constant light conditions, in fluctuating light, we observed significantly stronger photoinhibition in the ptGLYK-GFP lines than in gGLYK-GFP (Figure 5E), indicating that cytoplasmic photorespiratory bypass mediated by cytGLYK alleviates fluctuating light-induced photoinhibition.

Next, we investigated the accumulation of cytGLYK proteins under natural conditions. In wild-type plants, endogenous cytGLYK proteins accumulated in response to simulated shade using a low-red/far-red light ratio, whereas *phyAphyB* double mutants accumulated cytGLYK proteins regardless of the light conditions (Figure 6A). Consistent changes in the alternative promoter selection of *GLYK* (Figure 6B) and those in the *cytGLYK* transcript levels (Figures 6C and 6D) were confirmed in these conditions by 5′ RACE and RT-PCR, respectively. These results indicate that plants sense shade from other plants by inactivating phytochrome to accumulate cytGLYK proteins through alternative promoter selection. In the shade, plants have an increased probability of being exposed to fluctuating sunbeams streaming through the foliage (Sellaro et al., 2011). Thus, we speculate that, through phytochrome-mediated alternative promoter selection, plants accumulate cytGLYK proteins in the shade to prepare for the anticipated damage caused by light fluctuations.

Concluding Remarks

Based on the present findings, we conclude that phytochrome induces genome-wide changes in alternative promoter selection to modulate protein localization, thereby allowing plants to adapt to light environments. Plastidial proteins are the main targets of this regulatory mechanism, which is consistent with the observations that phytochrome regulates most chloroplastic functions, including various aspects of photosynthesis (Berry et al., 2013; Oh and Montgomery, 2014). Although the phenomenon of alternative promoter selection itself is already known, the impact of this mechanism on the proteome and its biological significance in general context has been underestimated. Our results not only show that alternative promoter selection constitutes a fundamental mechanism used by plants to adapt to light environments, but also strongly suggest that alternative promoter usage substantially contributes to the functional diversification of the proteome by allowing a single protein to perform different functions in different cellular compartments. Given that changes in alternative promoter selection on a similar scale could potentially be induced by signals other than phytochrome, alternative promoter selection likely represents another ubiquitous layer of gene expression regulation in eukaryotes that produces a more complex proteome and thereby imparts a higher level of adaptability.

STAR★METHODS

Detailed methods are provided in the online version of this paper and include the following:

- KEY RESOURCES TABLE
- CONTACT FOR REAGENT AND RESOURCE SHARING
- EXPERIMENTAL MODEL AND SUBJECT DETAILS
  - Arabidopsis

SUPPLEMENTAL INFORMATION

Supplemental Information includes five figures, six tables, and one data file and can be found with this article online at https://doi.org/10.1016/j.cell.2017.10.018.

AUTHOR CONTRIBUTIONS

T.U., K.H., M.T., Y.Y.Y., and T.M. conceived and designed the study. T.U., E.G., W.Y., Y.K., H.T., M.K., Y.S., and T.M. performed experiments. K.H. and A.F. analyzed the data. Y.T. provided intellectual input. T.U., K.H., and T.M. wrote the manuscript. All authors discussed the results and revised the manuscript.

ACKNOWLEDGMENTS

We thank T. Shikanai for critical reading of the manuscript; K. Abe for the TSS-seq experiment; K. Hikosaka, T. Furumoto, M. Hirai, M. Tsuyama, and A. Makino for valuable discussions; S. Inoue for anti-PHOT1 antibody; T. Ueda for *tagRFP* clone; N. Koike and R. Kunihiro for technical assistance; and the National Institute of Genetics for providing supercomputer services. This work was supported by JST CREST grant number JPMJCR11B3 (to K.H.), ALCA (to Y.Y.Y.), and PRESTO grant numbers JPMJPR13BB (to W.Y.), JPMJPR13B5 (to M.K.), and JPMJPR13B9 (to T.M.); JSPS KAKENHI grant numbers JP25120720, JP16H01470, JP16H04808, JP16H06279, and JP17H05727 (to T.M.), JP15K14421 (to K.H.), and JP16H06552 (to W.Y.); and a research grant from Takeda Science Foundation (to T.M.).

Received: July 30, 2017
Revised: September 15, 2017
Accepted: October 12, 2017
Published: November 9, 2017

REFERENCES

Barrera, L.O., Li, Z., Smith, A.D., Arden, K.C., Cavenee, W.K., Zhang, M.Q., Green, R.D., and Ren, B. (2008). Genome-wide mapping and analysis of active promoters in mouse embryonic stem cells and adult organs. Genome Res. *18*, 46–59.

Berry, J.O., Yerramsetty, P., Zielinski, A.M., and Mure, C.M. (2013). Photosynthetic gene expression in higher plants. Photosynth. Res. *117*, 91–120.

Boldt, R., Edner, C., Kolukisaoglu, U., Hagemann, M., Weckwerth, W., Wienkoop, S., Morgenthal, K., and Bauwe, H. (2005). D-GLYCERATE 3-KINASE, the last unknown enzyme in the photorespiratory cycle in Arabidopsis, belongs to a novel kinase family. Plant Cell *17*, 2413–2420.

Casal, J.J. (2013). Photoreceptor signaling networks in plant responses to shade. Annu. Rev. Plant Biol. *64*, 403–427.

Clough, S.J., and Bent, A.F. (1998). Floral dip: a simplified method for *Agrobacterium*-mediated transformation of *Arabidopsis thaliana*. Plant J. *16*, 735–743.

Davuluri, R.V., Suzuki, Y., Sugano, S., Plass, C., and Huang, T.H. (2008). The functional consequences of alternative promoter use in mammalian genomes. Trends Genet. *24*, 167–177.

Franklin, K.A., and Quail, P.H. (2010). Phytochrome functions in Arabidopsis development. J. Exp. Bot. *61*, 11–24.

Galvão, V.C., and Fankhauser, C. (2015). Sensing the light environment in plants: photoreceptors and early signaling steps. Curr. Opin. Neurobiol. *34*, 46–53.

Hartmann, L., Drewe-Boß, P., Wießner, T., Wagner, G., Geue, S., Lee, H.C., Obermüller, D.M., Kahles, A., Behr, J., Sinz, F.H., et al. (2016). Alternative splicing substantially diversifies the transcriptome during early photomorphogenesis and correlates with the energy availability in Arabidopsis. Plant Cell *28*, 2715–2734.

Inoue, S., Kinoshita, T., Matsumoto, M., Nakayama, K.I., Doi, M., and Shimazaki, K. (2008). Blue light-induced autophosphorylation of phototropin is a primary step for signaling. Proc. Natl. Acad. Sci. USA *105*, 5626–5631.

Jung, J.H., Domijan, M., Klose, C., Biswas, S., Ezer, D., Gao, M., Khattak, A.K., Box, M.S., Charoensawan, V., Cortijo, S., et al. (2016). Phytochromes function as thermosensors in Arabidopsis. Science *354*, 886–889.

King, B.R., and Guda, C. (2007). ngLOC: an *n*-gram-based Bayesian method for estimating the subcellular proteomes of eukaryotes. Genome Biol. *8*, R68.

Kodama, Y. (2016). Time gating of chloroplast autofluorescence allows clearer fluorescence imaging in planta. PLoS ONE *11*, e0152484.

Kornblihtt, A.R. (2005). Promoter usage and alternative splicing. Curr. Opin. Cell Biol. *17*, 262–268.

Kusano, M., Fukushima, A., Arita, M., Jonsson, P., Moritz, T., Kobayashi, M., Hayashi, N., Tohge, T., and Saito, K. (2007). Unbiased characterization of genotype-dependent metabolic regulations by metabolomic approach in *Arabidopsis thaliana*. BMC Syst. Biol. *1*, 53.

Landry, J.R., Mager, D.L., and Wilhelm, B.T. (2003). Complex controls: the role of alternative promoters in mammalian genomes. Trends Genet. *19*, 640–648.

Langmead, B., and Salzberg, S.L. (2012). Fast gapped-read alignment with Bowtie 2. Nat. Methods *9*, 357–359.

Leivar, P., and Monte, E. (2014). PIFs: systems integrators in plant development. Plant Cell *26*, 56–78.

Mancini, E., Sanchez, S.E., Romanowski, A., Schlaen, R.G., Sanchez-Lamas, M., Cerdán, P.D., and Yanovsky, M.J. (2016). Acute effects of light on alternative splicing in light-grown plants. Photochem. Photobiol. *92*, 126–133.

Matsushita, T., Mochizuki, N., and Nagatani, A. (2003). Dimers of the N-terminal domain of phytochrome B are functional in the nucleus. Nature *424*, 571–574.

Mejía-Guerra, M.K., Li, W., Galeano, N.F., Vidal, M., Gray, J., Doseff, A.I., and Grotewold, E. (2015). Core promoter plasticity between maize tissues and genotypes contrasts with predominance of sharp transcription initiation sites. Plant Cell *27*, 3309–3320.

Menon, C., Sheerin, D.J., and Hiltbrunner, A. (2016). SPA proteins: SPAnning the gap between visible light and gene expression. Planta *244*, 297–312.

Morton, T., Petricka, J., Corcoran, D.L., Li, S., Winter, C.M., Carda, A., Benfey, P.N., Ohler, U., and Megraw, M. (2014). Paired-end analysis of transcription

start sites in Arabidopsis reveals plant-specific promoter signatures. Plant Cell *26*, 2746–2760.

Myouga, F., Motohashi, R., Kuromori, T., Nagata, N., and Shinozaki, K. (2006). An Arabidopsis chloroplast-targeted Hsp101 homologue, APG6, has an essential role in chloroplast development as well as heat-stress response. Plant J. *48*, 249–260.

Nagatani, A., and Matsushita, T. (2002). Light-induced nuclear targeting of phytochromeB-sgreen fluorescent protein in plants. Methods Mol. Biol. *183*, 163–170.

Oh, S., and Montgomery, B.L. (2014). Phytochrome-dependent coordinate control of distinct aspects of nuclear and plastid gene expression during anterograde signaling and photomorphogenesis. Front. Plant Sci. *5*, 171.

Ohmiya, H., Vitezic, M., Frith, M.C., Itoh, M., Carninci, P., Forrest, A.R., Hayashizaki, Y., Lassmann, T., and The FANTOM Consortium (2014). RECLU: a pipeline to discover reproducible transcriptional start sites and their alternative regulation using capped analysis of gene expression (CAGE). BMC Genomics *15*, 269.

Osaki, Y., and Kodama, Y. (2017). Particle bombardment and subcellular protein localization analysis in the aquatic plant *Egeria densa*. PeerJ *5*, e3779.

Peterhansel, C., Horst, I., Niessen, M., Blume, C., Kebeish, R., Kürkcüoglu, S., and Kreuzaler, F. (2010). Photorespiration. Arabidopsis Book *8*, e0130.

Redestig, H., Fukushima, A., Stenlund, H., Moritz, T., Arita, M., Saito, K., and Kusano, M. (2009). Compensation for systematic cross-contribution improves normalization of mass spectrometry based metabolomics data. Anal. Chem. *81*, 7974–7980.

Redestig, H., Kusano, M., Fukushima, A., Matsuda, F., Saito, K., and Arita, M. (2010). Consolidating metabolite identifiers to enable contextual and multiplatform metabolomics data analysis. BMC Bioinformatics *11*, 214.

Reed, J.W., Nagpal, P., Poole, D.S., Furuya, M., and Chory, J. (1993). Mutations in the gene for the red/far-red light receptor phytochrome B alter cell elongation and physiological responses throughout Arabidopsis development. Plant Cell *5*, 147–157.

Reed, J.W., Nagatani, A., Elich, T.D., Fagan, M., and Chory, J. (1994). Phytochrome A and phytochrome B have overlapping but distinct functions in Arabidopsis development. Plant Physiol. *104*, 1139–1149.

Rojas-Duran, M.F., and Gilbert, W.V. (2012). Alternative transcription start site selection leads to large differences in translation activity in yeast. RNA *18*, 2299–2305.

Sellaro, R., Yanovsky, M.J., and Casal, J.J. (2011). Repression of shade-avoidance reactions by sunfleck induction of *HY5* expression in Arabidopsis. Plant J. *68*, 919–928.

Shabalina, S.A., Spiridonov, A.N., Spiridonov, N.A., and Koonin, E.V. (2010). Connections between alternative transcription and alternative splicing in mammals. Genome Biol. Evol. *2*, 791–799.

Shikata, H., Hanada, K., Ushijima, T., Nakashima, M., Suzuki, Y., and Matsushita, T. (2014). Phytochrome controls alternative splicing to mediate light responses in Arabidopsis. Proc. Natl. Acad. Sci. USA *111*, 18781–18786.

Shinomura, T., Nagatani, A., Hanzawa, H., Kubota, M., Watanabe, M., and Furuya, M. (1996). Action spectra for phytochrome A- and B-specific photoinduction of seed germination in *Arabidopsis thaliana*. Proc. Natl. Acad. Sci. USA *93*, 8129–8133.

Small, I., Peeters, N., Legeai, F., and Lurin, C. (2004). Predotar: A tool for rapidly screening proteomes for N-terminal targeting sequences. Proteomics *4*, 1581–1590.

Suorsa, M., Järvi, S., Grieco, M., Nurmi, M., Pietrzykowska, M., Rantala, M., Kangasjärvi, S., Paakkarinen, V., Tikkanen, M., Jansson, S., and Aro, E.M. (2012). PROTON GRADIENT REGULATION5 is essential for proper acclimation of Arabidopsis photosystem I to naturally and artificially fluctuating light conditions. Plant Cell *24*, 2934–2948.

Takahashi, S., Bauwe, H., and Badger, M. (2007). Impairment of the photorespiratory pathway accelerates photoinhibition of photosystem II by suppression of repair but not acceleration of damage processes in Arabidopsis. Plant Physiol. *144*, 487–494.

Timm, S., Nunes-Nesi, A., Pärnik, T., Morgenthal, K., Wienkoop, S., Keerberg, O., Weckwerth, W., Kleczkowski, L.A., Fernie, A.R., and Bauwe, H. (2008). A cytosolic pathway for the conversion of hydroxypyruvate to glycerate during photorespiration in Arabidopsis. Plant Cell *20*, 2848–2859.

Tsuchihara, K., Suzuki, Y., Wakaguri, H., Irie, T., Tanimoto, K., Hashimoto, S., Matsushima, K., Mizushima-Sugano, J., Yamashita, R., Nakai, K., et al. (2009). Massive transcriptional start site analysis of human genes in hypoxia cells. Nucleic Acids Res. *37*, 2249–2263.

Wang, X., Hou, J., Quedenau, C., and Chen, W. (2016). Pervasive isoform-specific translational regulation via alternative transcription start sites in mammals. Mol. Syst. Biol. *12*, 875.

Wiesner, T., Lee, W., Obenauf, A.C., Ran, L., Murali, R., Zhang, Q.F., Wong, E.W., Hu, W., Scott, S.N., Shah, R.H., et al. (2015). Alternative transcription initiation leads to expression of a novel ALK isoform in cancer. Nature *526*, 453–457.

Wu, H.P., Su, Y.S., Chen, H.C., Chen, Y.R., Wu, C.C., Lin, W.D., and Tu, S.L. (2014). Genome-wide analysis of light-regulated alternative splicing mediated by photoreceptors in *Physcomitrella patens*. Genome Biol. *15*, R10.

Yamori, W., and Shikanai, T. (2016). Physiological functions of cyclic electron transport around photosystem I in sustaining photosynthesis and plant growth. Annu. Rev. Plant Biol. *67*, 81–106.

STAR★METHODS

KEY RESOURCES TABLE

REAGENT or RESOURCE	SOURCE	IDENTIFIER
Antibodies		
Rabbit polyclonal anti-RbcL	Agrisera	Cat#AS03 037
Mouse monoclonal anti-PHYB (clone mBA2)	Shinomura et al., 1996	N/A
Rabbit polyclonal anti-PHOT1	Inoue et al., 2008	N/A
Rabbit polyclonal anti-totalGLYK	This paper	N/A
Rabbit polyclonal anti-cytGLYK	This paper	N/A
Goat anti-Mouse IgG (H + L)-HRP Conjugate	BIO-RAD	Cat#170-6516
Goat anti-Rabbit IgG (H + L)-HRP Conjugate	BIO-RAD	Cat#170-6515
Chemicals, Peptides, and Recombinant Proteins		
bacterial alkaline phosphatase (BAP)	TaKaRa	Cat#2120A
Cap-Clip Acid Pyrophosphatase	CELLSCRIPT	Cat#C-CC15011H
T4 RNA ligase	TaKaRa	Cat#2050A
DNase I	TaKaRa	Cat#2270A
ExTaq HS DNA Polymerase	TaKaRa	Cat#RR006A
Critical Commercial Assays		
μMACS Oligo(dT) MicroBeads	Miltenyi Biotec	Cat#120-002-541
SuperScript II	Invitrogen	Cat#18064-014
Phusion PCR Kit	NEB	Cat#F-531
SMARTer RACE 5′/3′ Kit	Clontech	Cat#634859
Verso cDNA synthesis Kit	Thermo Fisher Scientific	Cat#AB1453A
Agilent DNA 7500 Kit	Agilent	Cat#5067-1506
Agilent DNA 1000 Kit	Agilent	Cat#5067-1504
Deposited Data		
TSS-seq raw data	This paper	GenBank: DRA005891
Experimental Models: Organisms/Strains		
Arabidopsis: *phyA-211*	Reed et al., 1994	N/A
Arabidopsis: *phyB-9*	Reed et al., 1993	N/A
Arabidopsis: *glyk1-1*	Boldt et al., 2005	SALK_085479
Arabidopsis: gGLYK-GFP	This paper	N/A
Arabidopsis: ptGLYK-GFP	This paper	N/A
Arabidopsis: cytGLYK-GFP	This paper	N/A
Oligonucleotides		
Primers for 5′ RACE, see Table S6	This paper	N/A
Primer for RT-PCR: GLYK FW: TTCGAACCC ATTCCTCTTTC	This paper	N/A
Primer for RT-PCR: GLYK RV: TGACACCGA AGAGACATCCA	This paper	N/A
Primer for RT-PCR: cytGLYK FW: TTCGAAC CCATTCCTCTTTC	This paper	N/A
Recombinant DNA		
pBIN30/*gGLYK-GFP*-nosT	This paper	N/A
pBIN30/*gGLYK(Δ2ndATG)-GFP*-nosT	This paper	N/A
pBIN30/masP-*cytGLYK-GFP*-nosT	This paper	N/A
pAN19/35S-*tagRFP*-nosT	This paper	N/A

(*Continued on next page*)

Continued		
REAGENT or RESOURCE	SOURCE	IDENTIFIER
pGWT35S-*RBCS1A(1–79)-tagRFP*-nosT	Osaki and Kodama, 2017	N/A
pAN19/35S-*AT1G80380(Long)-GFP*-nosT	This paper	N/A
pAN19/35S-*AT1G80380(Short)-GFP*-nosT	This paper	N/A
pAN19/35S-*AT3G02040(Long)-GFP*-nosT	This paper	N/A
pAN19/35S-*AT3G02040(Short)-GFP*-nosT	This paper	N/A
pAN19/35S-*AT4G04960(Long)-GFP*-nosT	This paper	N/A
pAN19/35S-*AT4G04960(Short)-GFP*-nosT	This paper	N/A
pAN19/35S-*AT4G34120(Long)-GFP*-nosT	This paper	N/A
pAN19/35S-*AT4G34120(Short)-GFP*-nosT	This paper	N/A
pAN19/35S-*AT5G44650(Long)-GFP*-nosT	This paper	N/A
pAN19/35S-*AT5G44650(Short)-GFP*-nosT	This paper	N/A
pAN19/35S-*AT5G53930(Long)-GFP*-nosT	This paper	N/A
pAN19/35S-*AT5G53930(Short)-GFP*-nosT	This paper	N/A
Software and Algorithms		
SPSS	IBM Analytics	N/A
R (Version 3.4.0)	R Core Team	https://cran.r-project.org
Trim Galore! (Version 0.4.4)	Felix Krueger	http://www.bioinformatics.babraham.ac.uk/projects/trim_galore/
Bowtie2 (Version 2.3.0)	Langmead and Salzberg, 2012	http://bowtie-bio.sourceforge.net/bowtie2/index.shtml
RECLU (reclu 1.0)	Ohmiya et al., 2014	https://osdn.net/projects/reclu/
Q-value (Version 2.1.1)	John D. Storey	https://github.com/jdstorey/qvalue
ngLOC (v1.0)	King and Guda, 2007	http://genome.unmc.edu/ngLOC/
Predotar (version 1.04)	Small et al., 2004	https://urgi.versailles.inra.fr/predotar/
CCMN method	Redestig et al., 2009	N/A
MetMask	Redestig et al., 2010	http://metmask.sourceforge.net
Other		
Light Meter	LI-COR	LI-250A
2100 Bioanalyzer	Agilent	Model G2939A
HiSeq 2500	Illumina	Cat#SY-401-2501
Biolistic PDS-1000/He Particle Delivery System	BIO-RAD	Cat#165-2257
Confocal laser scanning microscope	Olympus	FV10i
White Light Laser Confocal Microscope	Leica Microsystems	TCS SP8 X
Portable photosynthesis system	LI-COR	LI-6400
Imaging-PAM M-Series, Maxi version	Heinz Walz	Model: IMAG-MAX/L

CONTACT FOR REAGENT AND RESOURCE SHARING

Further information and requests for resources and reagents should be directed to and will be fulfilled by the Lead Contact, Tomonao Matsushita (mat@agr.kyushu-u.ac.jp).

EXPERIMENTAL MODEL AND SUBJECT DETAILS

Arabidopsis

The *Arabidopsis thaliana* mutant alleles used in this study were *phyA-211* (Reed et al., 1994), *phyB-9* (Reed et al., 1993), and *glyk1-1* (Boldt et al., 2005), all of which were in Columbia (Col) background. Surfaced-sterilized seeds were sown on 0.6% agar plates containing Murashige and Skoog medium without sucrose. The plates were kept in darkness for at least 3 days and then irradiated with continuous white light (40 μmol m^{-2} s^{-1}) for 3–4 hr at 22°C to induce germination. The plates were then placed at 22°C under the light conditions specified in each figure legend.

The genomic DNA fragment of *GLYK* (*gGLYK*) that includes the promoter region and the transcribed region without the stop codon was fused in-frame to the 5′ end of the *sGFP* gene. This construct was inserted into pBIN30/nosT to obtain

pBIN30/*gGLYK-GFP*-nosT, and *glyk* null mutants were transformed with this plasmid using the *Agrobacterium*-mediated floral dip method (Clough and Bent, 1998) to generate the gGLYK-GFP line.

The second ATG of the *GLYK* coding sequence in pBIN30/*gGLYK-GFP*-nosT was mutated to TTG to block the translation of cytGLYK, and this mutated plasmid, pBIN30/*gGLYK(Δ2ndATG)-GFP*-nosT, was also transformed into *glyk* null mutants to generate the ptGLYK-GFP line, which accumulates only ptGLYK proteins. The cDNA fragment of *cytGLYK,* fused to the 5′ end of *sGFP*, was inserted between the constitutive *Agrobacterium tumefaciens* mannopine synthase promoter (masP) and the Nos terminator of pBIN30/masP-nosT. The resultant plasmid, pBIN30/masP-*cytGLYK-GFP*-nosT, was also introduced into *glyk* null mutants to generate the cytGLYK-GFP line, in which only cytGLYK proteins are constitutively expressed.

For each construct, more than 50 independent T2 lines that segregated at a 3:1 ratio for Basta-resistance were established, and two representative lines were chosen for analysis, based on the accumulation level of the introduced protein.

METHOD DETAILS

Light Conditions

The white light was directly from fluorescent tubes (FLR40SW/M, Mitsubishi) and the red light was from fluorescent tubes (FL20S/R, National) through a 3-mm thick, red-colored acrylic plate (SHINKOLITE A102, Mitsubishi Rayon), as previously reported (Matsushita et al., 2003). High R:FR light (15 μmol m^{-2} s^{-1} red light and 5 μmol m^{-2} s^{-1} far-red light) and low R:FR light (0.75 μmol m^{-2} s^{-1} red light and 2.5 μmol m^{-2} s^{-1} far-red light) were provided by light-emitting diodes with emission maxima at 660 nm and 735 nm, respectively. The fluence rates were measured with an optical power meter (Model LI-250A, LI-COR).

RNA Preparation and Transcription Start Site (TSS)-Sequencing Analysis

Fifty micrograms of total RNA extracted as previously reported (Shikata et al., 2014) was used for cap-replacement followed by sequencing library preparation, as follows. RNA was treated with 2.5 U bacterial alkaline phosphatase (BAP) (TaKaRa) at 37°C for 1 hr and then with 40 U Cap-Clip Acid Pyrophosphatase (CELLSCRIPT) at 37°C for 1 hr. The RNA was then ligated to 1.2 μg of the RNA oligonucleotide 5′-AAUGAUACGGCGACCACCGAGAUCUACACUCUUUCCCUACACGACGCUCUUCCGAUCUGG-3′ using 250 U T4 RNA ligase (TaKaRa) at 20°C for 3 hr. After DNase I treatment (TaKaRa), polyA-containing RNA was selected with μMACS Oligo(dT) MicroBeads (Miltenyi Biotec). The first-strand cDNA was synthesized by incubating the polyA-containing RNA with 10 pmol random hexamer primer (5′-CAAGCAGAAGACGGCATACGANNNNNNC-3′) using SuperScript II (Invitrogen), at 12°C for 1 hr and then at 42°C overnight. The template RNA was degraded by alkaline treatment. For PCR, 20% of the first-strand cDNA was used as the PCR template. PCR amplification was performed using the Phusion PCR Kit (NEB) with the PCR primers 5′-AATGATACGGCGACCACCGAG-3′ and 5′-CAAGCAGAAGACGGCATACGA-3′ under the following reaction conditions: 15 cycles at 94°C for 1 min, 56°C for 1 min, and 72°C for 2 min. The PCR fragments were size-fractionated by electrophoresis on a 12% polyacrylamide gel, and the fraction that contained 150–250 bp fragments was recovered. The quality and quantity of the obtained single-stranded first-strand cDNAs were assessed using a Bioanalyzer (Agilent). One nanogram of the size-fractionated cDNA was used for sequencing reactions with the Illumina HiSeq 2500 to generate 36-bp single-end reads. Sequencing was performed according to the manufacturer's instructions. Two replicates were independently prepared for each analysis.

Mapping and Clustering of TSS-Sequencing Reads

A total of 27.8-GB reads were determined by TSS-sequencing. The number of reads is shown in Figure S1A. Approximately 15.2% of reads with low-quality scores or adapters were partially trimmed using Trim Galore! (http://www.bioinformatics.babraham.ac.uk/projects/trim_galore/). The trimmed sequences were mapped to the *Arabidopsis* genome (The *Arabidopsis* Information Resource, TAIR10; http://www.arabidopsis.org/) with Bowtie2 software (http://bowtie-bio.sourceforge.net/bowtie2/index.shtml) (Langmead and Salzberg, 2012). The mapped sites were clustered for each experimental condition using the RECLU program to infer TSS peaks (Ohmiya et al., 2014) (TPM score > 0.1, IDR score > 0.1). When TSS peaks overlap with ≥ 1 bp in at least two of the five samples (see below), those TSS peaks are unified and re-defined as one TSS peak (Figure S1C). After this process, TSS peaks are defined to be "non-redundant." Non-redundant TSS peaks are referred to as "TSSs" in this study. TSSs were defined to belong to the corresponding gene when a TSS exists between the region 500-bp upstream of the representative TSS and the midpoint between the representative TSS and the transcription termination site (Morton et al., 2014). Out of the 40,709 non-redundant TSS peaks identified, 23,955 were assigned in annotated genes.

Comparison between TSS-seq and mRNA-seq

The number of mapped reads in each corresponding gene was defined as the total number of reads that were mapped in the region from 500-bp upstream of the representative TSS to the midpoint between the representative TSS and transcription termination site. The expression level inferred by TSS-seq and mRNA-seq is defined as the number of reads per million mapped reads and the number of reads per kilobase of exon model per million mapped reads (RPKM), respectively, for each corresponding gene.

Analysis of Phytochrome-Regulated Alternative Promoter Selection

When more than one TSS was assigned to an annotated coding gene, the gene has the potential to have alternative promoters. There were 6,143 genes with multiple TSSs. Phytochrome-regulated alternative promoter selection was determined based on the number of mapped TSS-seq reads in each TSS in the following five samples (genotype_exposure time in red light): WT_0h, WT_1h, WT_3h, *phyAphyB*_1h, and *phyAphyB*_3h (Figure 1A). The ratio of TSS-seq reads in each pair of alternative TSSs was compared among the five samples, and tested by the χ^2 test. From the estimated *P values*, the false discovery rate was inferred using *Q*-value software (https://github.com/jdstorey/qvalue). Then, alternative promoter selection was defined as being regulated by phytochrome, if the ratio of TSS-seq reads between each pair of alternative TSSs significantly changed, in response to red light and in a phytochrome-dependent manner, in the same direction at the same time (for each of the double statistical tests, FDR < 0.05, χ^2 test) (Figure S1D).

Bioinformatics Analysis of Protein Sequences Derived from TSSs

When TSSs existed in the 5′ upstream region of the representative start codons annotated by TAIR, coding nucleotide sequences derived from the upstream TSSs were generated to deduce protein sequences. In cases where stop codons appeared between the upstream TSS and the representative start codon, the first "ATG" downstream of the stop codon was defined as being the start codon for the transcript. When TSSs existed in the 3′ downstream regions of the representative start codons, the first "ATG" downstream of the 3′ TSS was defined as being the start codon for the transcript.

After predicting the protein sequences encoded by the nucleotide sequences, subcellular localization of the encoded proteins was inferred from the putative protein sequences using ngLOC software (King and Guda, 2007).

GO assignments were obtained from TAIR (http://www.arabidopsis.org/). GO terms in the cellular components category were analyzed. In each of the GO term subcategories, the χ^2 test was conducted to examine whether the ratio of the number of genes that encode protein isoforms with different N-terminal ends via phytochrome-controlled alternative promoter selection was significantly higher than the ratio of those genes in the genome. To correct for multiple testing, the moderated *P value* was estimated from a raw χ^2 test using *Q*-value software (https://github.com/jdstorey/qvalue).

Plastid transit peptides of protein sequences were inferred by two approaches (Small et al., 2004; Myouga et al., 2006).

5′ RACE Analysis

One microgram of the total RNA obtained was used for the 5′ rapid amplification of cDNA ends (5′ RACE) analysis, which was performed using the SMARTer RACE 5′/3′ Kit (Clontech) according to the manufacturer's instructions. The obtained cDNA was subjected to 5′-RACE PCR using ExTaq HS DNA Polymerase (TaKaRa). Gene-specific primers and number of PCR cycles are shown in Table S6. Quantification of the amounts of transcripts from phytochrome-controlled alternative promoters was performed with the Agilent DNA 7500 Kit and 2100 Bioanalyzer (Agilent), according to the manufacturer's instructions. The specific bands were confirmed by sequencing all the bands in each reaction.

RT-PCR Analysis

cDNA was synthesized using the Verso cDNA synthesis Kit (Thermo Fisher Scientific) according to the manufacturer's instructions. The obtained cDNA was subjected to reverse transcription PCR (RT-PCR) using ExTaq HS DNA Polymerase (TaKaRa). The primers used and number of PCR cycles were as follows: *cytGLYK*, 5′-TTCGAACCCATTCCTCTTTC-3′ (FW) and 5′-TGACACCGAAGAGA CATCCA-3′ (RV), 25 cycles; *TUB2* (*AT5G62690*), 5′-ATCCGGTGCTGGTAACAACT-3′ (FW) and 5′-ATCCAGTTCCTCCTCCCAAC-3′ (RV), 25 cycles. DNA concentrations of the PCR products were quantified with the Agilent DNA 1000 Kit and 2100 Bioanalyzer (Agilent), according to the manufacturer's instructions.

Confocal Microscopy Observation of Subcellular Localization in Onion Epidermal Cells

cDNA fragments of each gene without stop codons were fused in-frame to the 5′ end of the *sGFP* gene, and these fusion constructs were inserted between the constitutive cauliflower mosaic virus 35S promoter and the Nos terminator of pAN19/35S-nosT. To express marker proteins, *tagRFP* alone and *tagRFP* fused in-frame to the 3′ end of the DNA fragment encoding the plastid transit peptide of RBCS1A (amino acid residues 1–79) were inserted into pAN19/35S-nosT and pGWT35S-nosT, respectively (Osaki and Kodama, 2017). Cells in the epidermal layer of onion bulbs were transformed by particle bombardment (PDS-1000/He, BIO-RAD) essentially as described (Nagatani and Matsushita, 2002), except that spring onions were used immediately after harvest, which dramatically reduced autofluorescence of the samples. After bombardment, the tissue was incubated for 12 hr at 22°C under continuous white light (40 μmol m^{-2} s^{-1}). The subcellular localization of the GFP and tagRFP fluorescence was visualized using a confocal laser scanning microscope (FV10i, Olympus) with an excitation laser at 473 nm (green: GFP) and at 559 nm (red: tagRFP). For each construct, transfections were repeated at least five times, a minimum of 100 cells were analyzed from each experiment, and the GFP localization patterns observed in more than 90% of the transfected cells are shown.

Confocal Microscopy Observation of Subcellular Localization in *Arabidopsis*

Seeds of wild-type (Col-0) and transgenic plants (gGLYK-GFP, ptGLYK-GFP, and cytGLYK-GFP) were sown on Murashige and Skoog medium with 0.8% agar, and grown under continuous white light (70 μmol m^{-2} s^{-1}) from light-emitting diodes

(Tube-120, Ekou) at 22°C in a cultivation room. After 3 weeks, the plants were analyzed as light-treated samples using a confocal microscope SP8X (Leica Microsystems). For dark treatment, 3-week-old plants were incubated for 24–72 hr in a steel box in the cultivation room.

For analysis of intact mesophyll cells, detached leaves were directly observed. To detect GFP fluorescence under rejection of chlorophyll autofluorescence, time-gated imaging using the HyD hybrid detector (Leica Microsystems) with a gating time of 0.5–12.0 nsec was employed (Kodama, 2016). For observation of chlorophyll autofluorescence, a conventional photomultiplier tube (PMT) was used. For imaging of GFP and chlorophyll autofluorescence, an excitation laser line at 485 nm was obtained from the white light laser (WLL, Leica Microsystems) and emission spectra at 490–550 nm and 620–685 nm were selected for GFP and chlorophyll autofluorescence, respectively.

To observe GFP fluorescence more clearly, protoplasts were prepared from mesophyll cells of the transgenic plants. After light or dark treatment, protoplasts were prepared. Briefly, a leaf was sandwiched between two strips of vinyl tape, and the lower epidermis was removed. The stripped leaf was treated with enzyme solution (1% cellulose R-10, 0.3% macerozyme R-10, 0.4 M mannitol, 20 mM KCl, 20 mM MES (pH 5.7), 10 mM $CaCl_2$) to release mesophyll protoplasts. The protoplast cells were isolated using a micropipette, and then directly observed.

Immunochemical Experiments

Total protein was extracted in a buffer containing 50 mM Tris-HCl (pH 7.5), 200 mM NaCl, 5 mM EDTA, 0.1% Triton X-100, 4 mM urea, and protease inhibitor cocktail (Sigma-Aldrich). The proteins were separated using SDS-PAGE and transferred to polyvinylidene fluoride membranes. Anti-totalGLYK and anti-cytGLYK polyclonal antibodies were raised in rabbits by subcutaneous injection of the synthetic peptides CRGDRADSSTWPEVEGPLS (corresponding to amino acid residues 219–236 of cytGLYK) and MVHDYATTTNGTSKRC (corresponding to amino acid residues 1–16 of cytGLYK), respectively (Sigma-Aldrich). Proteins were identified using anti-totalGLYK antibody, anti-cytGLYK antibody, anti-PHYB monoclonal antibody mBA2 (Shinomura et al., 1996), anti-PHOT1 polyclonal antibody (Inoue et al., 2008), and anti-RbcL (ribulose-1,5-bisphosphate carboxylase/oxygenase large subunit) polyclonal antibody (AS03 037, Agrisera).

Fractionation Experiments

The chloroplast fraction and chloroplast-excluded fraction were obtained from mesophyll cell protoplasts. Mesophyll cell protoplasts were isolated enzymatically from 4-week-old plants grown in continuous white light (40 μmol m^{-2} s^{-1}), and then suspended in 1 ml of 0.6 M mannitol buffer (pH 5.5) containing 1 mM $CaCl_2$, 1 mM $MgCl_2$, and 0.2% bovine serum albumin (BSA). The protoplasts were broken by pipetting with tips that had been attached to a 20 μm nylon mesh. The suspension was centrifuged at 400 × g for 5 min at 4°C, to separate the chloroplast pellet from the supernatant.

The chloroplast pellet was washed with 0.4 M sorbitol containing 50 mM HEPES-KOH (pH 7.6) and 1 mM EDTA, and used as the chloroplast fraction. The supernatant was centrifuged at 10,000 × g for 5 min at 4°C to remove contamination, and used as the chloroplast-excluded fraction.

Gas Exchange Analysis

Gas exchange of intact *Arabidopsis* leaves was measured with an open gas exchange system (LI-6400, LI-COR). Plants were kept in darkness for over 3 hours, and then measurements were performed at 30 min after the transfer from dark to white light conditions at controlled air temperature (22°C) and relative humidity (50%–60%).

Metabolome Analysis of Photorespiration

Gas chromatography time-of-flight mass spectrometry (GC-TOF-MS) was used for metabolite profiling as previously described (Kusano et al., 2007) with minor modifications. Briefly, each sample at a concentration of 25 mg FW/ml was extracted using extraction medium ($CHCl_3$:MeOH:H_2O; 2:6:2 (v/v/v)), including 10 stable isotope reference compounds. The sample extracts were then derivatized, i.e., subjected to methoxymation and silylation. One microliter of the derivatized sample (equivalent to 56 μg FW) was used for GC-TOF-MS analysis.

Chlorophyll Fluorescence Analysis

Chlorophyll fluorescence was measured with an imaging fluorometer (IMAGING-PAM; Heinz Walz) in plants grown at a light intensity of 150 μmol m^{-2} s^{-1} and a CO_2 concentration of 3,000 μmol mol^{-1} under a 12-hr light (22°C)/12-hr dark (20°C) photoperiod. These plants were first exposed for 10 min to a light intensity of 150 μmol m^{-2} s^{-1} at a CO_2 concentration of 3,000 μmol mol^{-1} to obtain the steady-state, and the quantum yield of electron transfer to PSII (ΦPSII) was measured at 5 min and 10 min after the changes in CO_2 concentration from 3,000 μmol mol^{-1} to 400 μmol mol^{-1} (Figure S5C).

Photoinhibition Analysis

Photoinhibition was analyzed using an IMAGING-PAM fluorometer after 24 hr of exposure to light with an intensity of 150 μmol m^{-2} s^{-1} and two different CO_2 concentrations (400 μmol mol^{-1} and 3,000 μmol mol^{-1}) in plants grown at a light intensity of 150 μmol m^{-2} s^{-1} and a CO_2 concentration of 3,000 μmol mol^{-1} under a 12-hr light (22°C)/12-hr dark (20°C) photoperiod (Figure S5D). Photoinhibition was

also analyzed after irradiating plants with constant high light (12-hr light/12-hr dark) or fluctuating light (3-min light/5-min dark), at 550 μmol m^{-2} s^{-1} for 2 days in plants grown at a light intensity of 150 μmol m^{-2} s^{-1} and CO_2 concentration of 400 μmol mol^{-1} under a 12-hr light (22°C)/12-hr dark (20°C) photoperiod (Figure 5E). The maximum quantum yield of PSII (Fv/Fm) after dark incubation for 20 min was measured before and after the light treatment.

QUANTIFICATION AND STATISTICAL ANALYSIS

SPSS software (IBM Analytics) was used for statistical analyses unless otherwise stated. No statistical methods were used to pre-determine sample size. All the center values are means of technical (Figures 2 and 6) or biological (all the other figures where applicable) replicates. For all the experiments, unless otherwise stated, the results shown are representative of experiments independently conducted at least three times that produced similar results. A Student's t test was used for comparison between two samples. Tukey–Kramer multiple comparison test was used for multiple comparisons. For metabolite profiling, data were normalized and summarized using the CCMN method (Redestig et al., 2009) and MetMask (Redestig et al., 2010), respectively. Significant changes in metabolite levels were determined by the Welch's t test using R statistical software (http://cran.r-project.org). All the statistical tests were two-sided tests.

DATA AND SOFTWARE AVAILABILITY

Data Resources

The accession number for the raw data files for the TSS-seq analysis reported in this paper is GenBank: DRA005891.

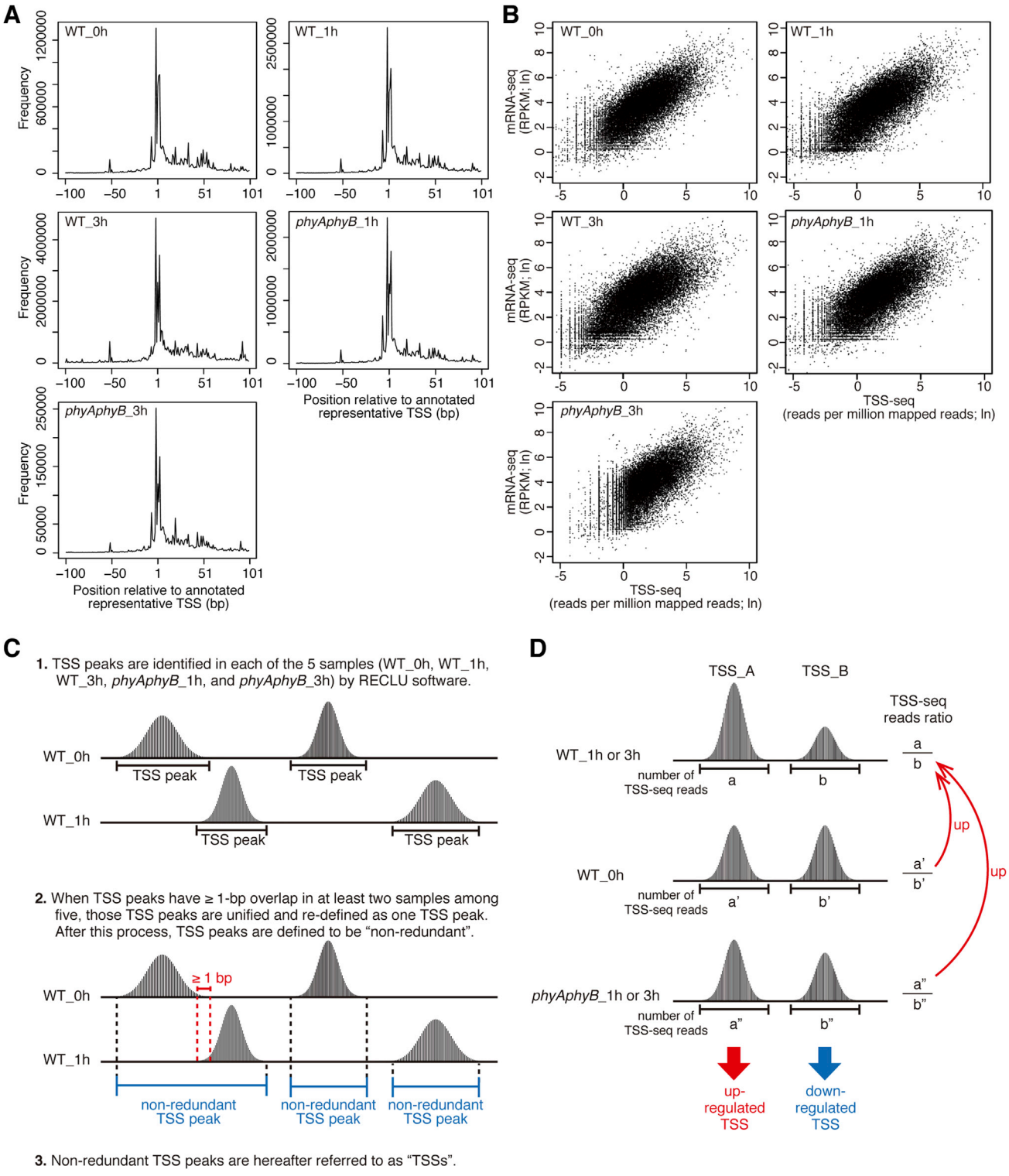

Figure S1. Analysis of Phytochrome-Regulated Alternative Promoter Selection, Related to Figure 1

(A) TSS positions relative to each representative annotated TSS. x axis shows genomic position relative to the representative TSS annotated in TAIR (= 1). y axis represents frequency of cumulative mapped TSS reads around representative TSSs at all the genes annotated in TAIR.

(B) Transcript levels inferred either from the TSS-seq data in reads per million mapped reads (x axis) or from the previous mRNA-seq data (Shikata et al., 2014) in reads per kilobase of exon model per million mapped reads (RPKM) (y axis).

(legend continued on next page)

(C) Identification and definition of TSSs in this work.

(D) Criteria of phytochrome-regulated alternative promoter selection. TSS_A and TSS_B are a pair of alternative TSSs within a gene locus. If both a/b > a'/b' and a/b > a"/b" are significantly fulfilled (FDR < 0.05, χ^2 test), then TSS_A and TSS_B are defined to be upregulated and downregulated, respectively, in phytochrome-controlled selection of alternative promoter.

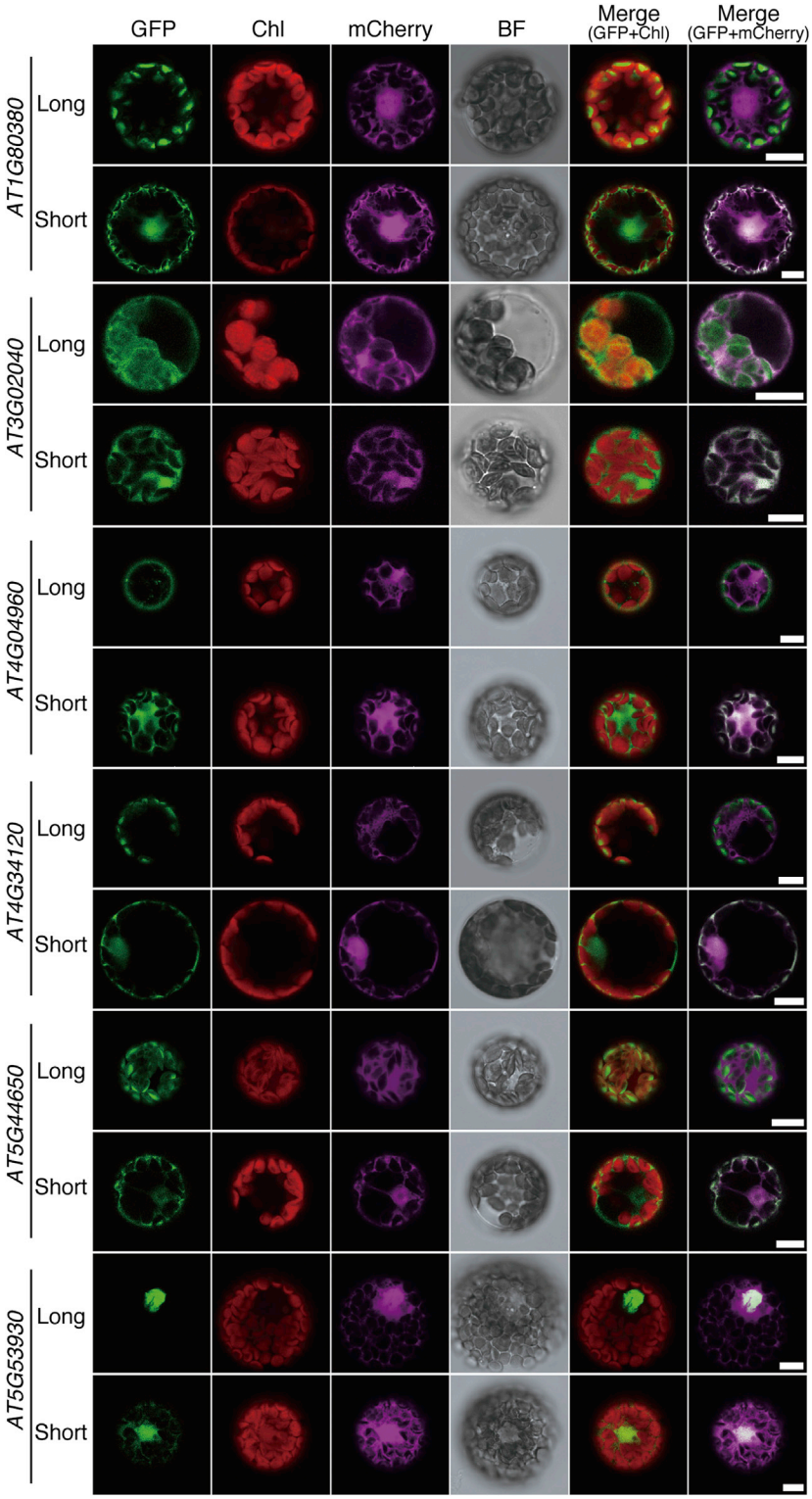

Figure S2. Phytochrome-Mediated Alternative Promoter Selection Produces Protein Isoforms with Different Subcellular Localizations, Related to Figure 3

Longer (Long) and shorter (Short) cDNAs resulting from phytochrome-mediated promoter selection were transiently expressed as fusion proteins with GFP in *Arabidopsis* mesophyll protoplasts by polyethylene glycol (PEG)-mediated transfection. mCherry alone was co-expressed to indicate the cytoplasm and nucleus. Chl, chlorophyll autofluorescence; BF, bright field. Scale bars, 10 μm.

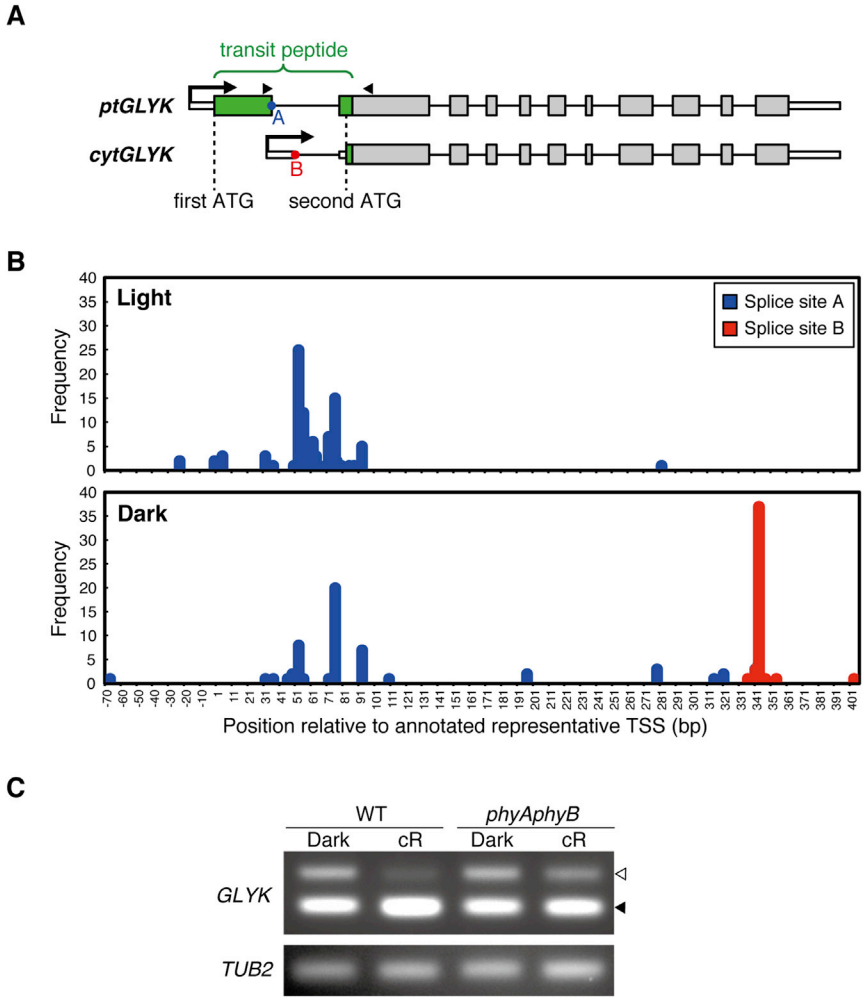

Figure S3. Alternative Promoter and Alternative Splicing of *GLYK*, Related to Figures 4 and 6

(A) Schematic illustration of *ptGLYK* and *cytGLYK* pre-mRNAs. A (in blue) and B (in red) indicate the first splice donor sites in *ptGLYK* and *cytGLYK* pre-mRNAs, respectively. The positions of the first and second ATGs of the *GLYK* coding sequence are also shown.

(B) Frequency distribution of TSS positions of the *GLYK* gene in light and dark conditions. Total RNA extracted from the shoots of 25-day-old wild-type plants grown in continuous white light (40 μmol m^{-2} s^{-1}) with or without 1 day of dark adaptation before sampling was used for 5′ RACE analysis. 5′-RACE PCR products were cloned and the TSS and position of the first splice donor site in each clone were determined. Genomic position relative to the representative TSS annotated in TAIR (= 1) is shown below.

(C) RT-PCR analysis of phytochrome-regulated alternative splicing of *GLYK*. The same RNA samples as in Figure 1D were analyzed. Black and white arrowheads indicate *ptGLYK* and *cytGLYK* transcripts, respectively. The primers used (FW: 5′-TTCGAACCCATTCCTCTTTC-3′; RV: 5′-TGACACCGAAGAGACATCCA-3′) are indicated by arrowheads in (A). *TUB2* was used as an internal control.

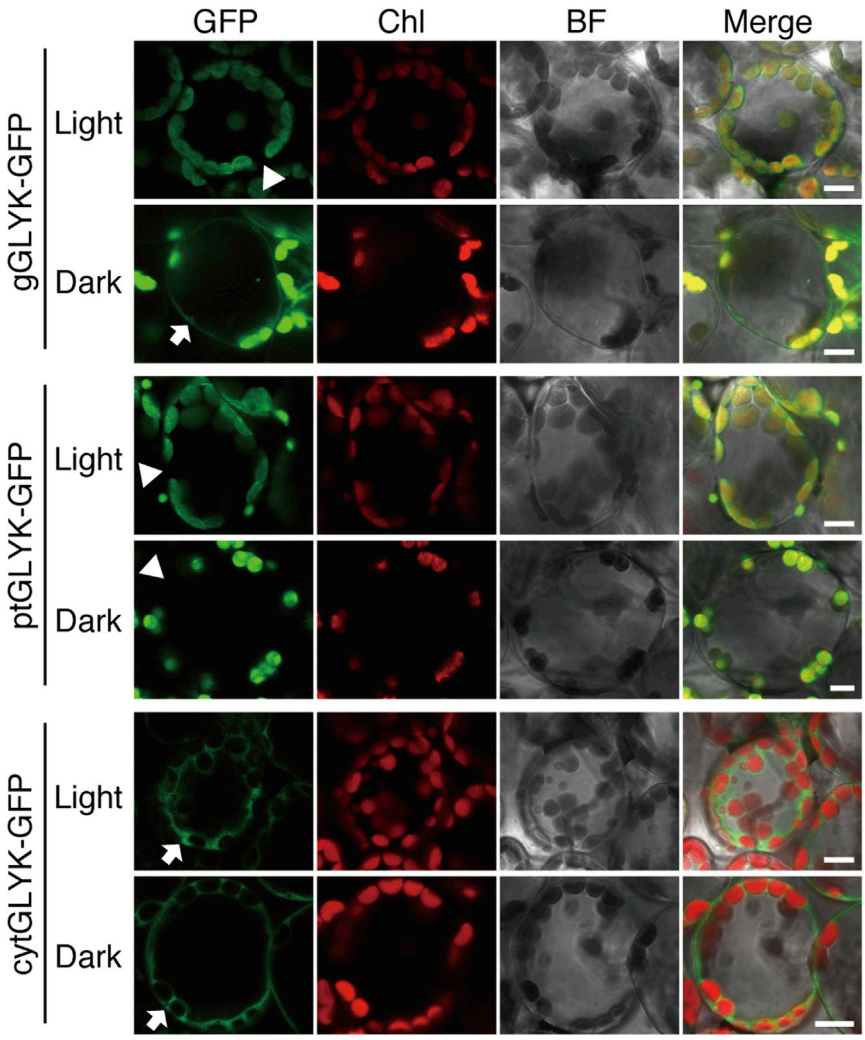

Figure S4. GLYK Shows Light-Dependent Changes in Subcellular Localization in Transgenic Plants, Related to Figure 4

Subcellular localization of GFP fluorescence in intact mesophyll cells of gGLYK-GFP, ptGLYK-GFP, and cytGLYK-GFP transgenic plants grown in continuous white light (70 μmol m^{-2} s^{-1}) and dark conditions. Arrows and arrowheads indicate the presence and absence of cytoplasmic GFP fluorescence, respectively. Chl, chlorophyll autofluorescence; BF, bright field. Scale bars, 10 μm.

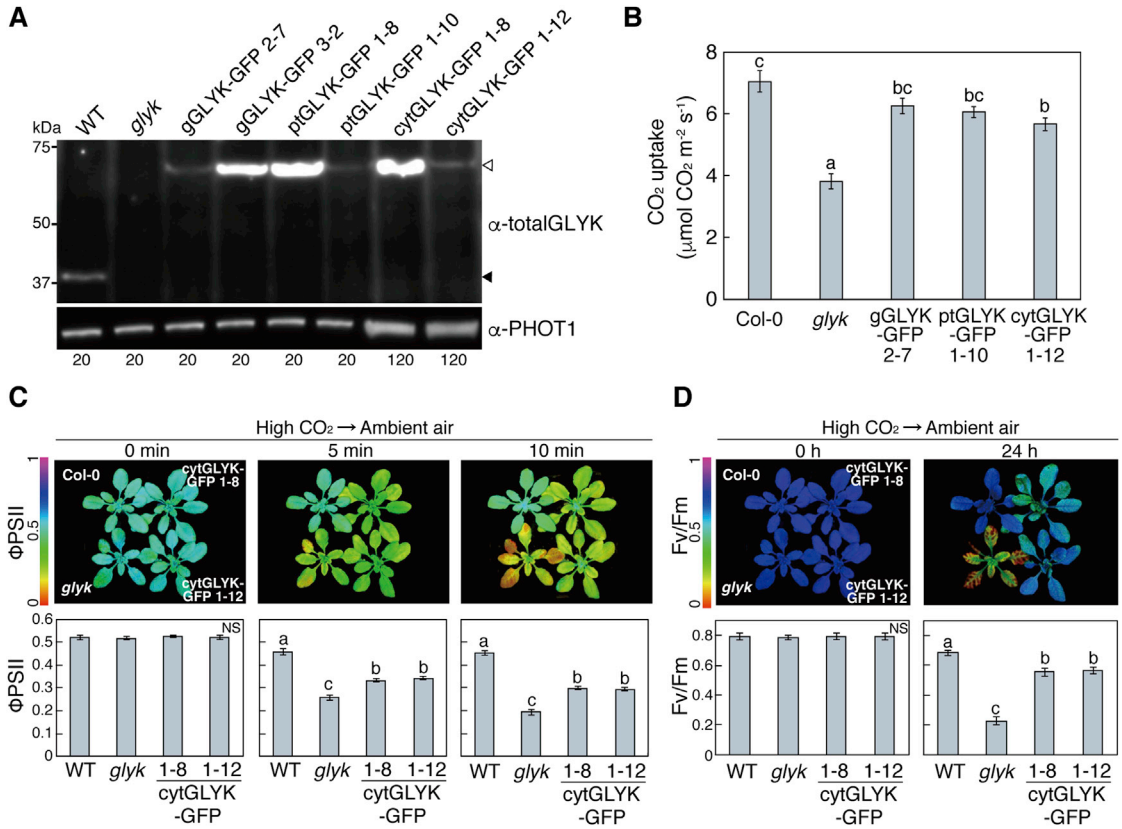

Figure S5. cytGLYK Constitutes Cytoplasmic Photorespiratory Bypass, Related to Figure 5

(A) Immunoblotting with anti-totalGLYK antibody. Anti-PHOT1 antibody was used as a loading control. Total protein was extracted from 4-day-old etiolated seedlings grown in ambient air. The amount of loaded total protein (in μg) is indicated beneath the blot. White and black arrowheads indicate introduced GLYK fused to GFP and endogenous GLYK, respectively.

(B) CO_2 uptake in response to light. CO_2 assimilation rate was measured after the transfer from dark to white light (300 μmol m^{-2} s^{-1}) conditions in plants grown for 4 weeks. Data are means ± SE of three independent experiments. Different letters indicate significantly different values ($p < 0.05$, Tukey-Kramer multiple comparison test).

(C and D) Quantum yield of electron transfer to PSII (ΦPSII) (C) and the degree of photoinhibition (D) were analyzed at the indicated time points after the CO_2 concentration was changed from 3,000 μmol mol^{-1} (high CO_2) to 400 μmol mol^{-1} (ambient air). Data are means ± SD (n = 3). Different letters indicate significantly different values ($p < 0.05$, Tukey-Kramer multiple comparison test). NS, not significant.